AGU Advances

Key Points:

- Pliocene sea-surface temperature (SST) data are assimilated with model simulations from pliocene modeling intercomparison project phase 2 (Plio-MIP2) and Community Earth System Model (CESM)
- The mid-Pliocene and early Pliocene were 4.1°C and 4.8°C warmer than preindustrial, respectively
- Reconstructed sea-surface salinity (SSS) is inconsistent with North Pacific Deep Water formation during the Pliocene

Supporting Information:

Supporting Information may be found in the online version of this article.

Correspondence to:

J. E. Tierney,
jesst@arizona.edu

Pliocene Warmth and Patterns of Climate Change Inferred From Paleoclimate Data Assimilation

Jessica E. Tierney[1] , Jonathan King[1,2] , Matthew B. Osman[3] , Jordan T. Abell[4] , Natalie J. Burls[5] , Ehsan Erfani[6] , Vincent T. Cooper[7] , and Ran Feng[8]

[1]Department of Geosciences, The University of Arizona, Tucson, AZ, USA, [2]United States Geological Survey, Golden, CO, USA, [3]Department of Geography, The University of Cambridge, Cambridge, UK, [4]Department of Earth & Environmental Sciences, Lehigh University, Bethlehem, PA, USA, [5]Department of Atmospheric, Oceanic and Earth Sciences, George Mason University, Fairfax, VA, USA, [6]Desert Research Institute, Reno, NV, USA, [7]Department of Atmospheric and Climate Science, University of Washington, Seattle, WA, USA, [8]Department of Geosciences, University of Connecticut, Storrs, CT, USA

Abstract As the last time period when CO_2 concentrations were near 400 ppm, the Pliocene Epoch (5.33–2.58 Ma) is a useful paleoclimate target for understanding future climate change. Existing estimates of global warming and climate sensitivity during the Pliocene rely mainly on model simulations. To reconstruct Pliocene climate and incorporate paleoclimate observations, we use data assimilation to blend sea-surface temperature (SST) proxies with model simulations from the Pliocene Modeling Intercomparison Project 2 and the Community Earth System Models. The resulting reconstruction, "plioDA," suggests that the mid-Pliocene (3.25 Ma) was warmer than previously thought (on average 4.1°C warmer than preindustrial, 95% CI = 3.0°C–5.3°C), leading to a higher estimate of climate sensitivity (4.8°C per doubling of CO_2, 90% CI = 2.6°C–9.9°C). In agreement with previous work, the tropical Pacific zonal SST gradient during the mid-Pliocene was moderately reduced (−0.8°C, 95% CI = −2.3–0.4°C). However, this gradient was more reduced during the early Pliocene (4.75 Ma, −2.3°C, 95% CI = −3.9–−1.1°C), a time period that is also warmer than the mid-Pliocene (4.8°C above preindustrial, 95% CI = 3.6°C–6.2°C). PlioDA reconstructs a fresh North Pacific and salty North Atlantic, supporting Arctic gateway closure and contradicting the presence of Pacific Deep Water formation. Overall, plioDA updates our view of global and spatial climate change during the Pliocene, as well as raising questions about the state of ocean circulation and the drivers of differences between the early and mid-Pliocene.

Plain Language Summary The last time CO_2 levels in the atmosphere approached 400 ppm was 3 million years ago, during the time called the Pliocene. Studying this time period can help us better understand near-future climate change. In this study, we combine geological observations of Pliocene SST with simulations of Pliocene climate conducted with climate models using a technique called data assimilation. The result is a map view of Pliocene climate called "plioDA." plioDA shows that Pliocene climate was warmer than previous work has indicated and therefore more sensitive to CO_2 changes. During the early Pliocene period in particular, the tropical Pacific was much warmer in the east than the west, similar to what we see today during an El Niño. plioDA suggests that it was rainier in the North Pacific and that the Indian-Asian monsoon system was stronger. Previous studies have suggested that the Pliocene had deep water formation in the North Pacific, much like the Atlantic today, but the salinity reconstruction in plioDA does not support this. Overall this study provides a new view of the main features of Pliocene climate, including an updated estimate of global temperature change, climate sensitivity, and the state of the ocean.

1. Introduction

The last time that Earth's atmospheric CO_2 concentrations exceeded 400 ppm was during the Pliocene epoch (5.33–2.58 Ma), a warm climate that preceded the cooling and growth of large Northern Hemisphere (NH) ice sheets during the Pleistocene (2.58–0.0117 Ma). Model simulations suggest that mid-Pliocene (ca. 3.2 Ma) global mean surface temperature (GMST) was on average ca. 3°C warmer than preindustrial conditions (Gulev et al., 2021; Haywood et al., 2020), and that the Greenland and West Antarctic ice sheets were much smaller (Golledge et al., 2017; Koenig et al., 2015), contributing to about 20 m of sea level rise (Dutton et al., 2015; Grant et al., 2019). In the tropical Pacific, the zonal SST gradient was reduced and Walker circulation weaker (Tierney, Haywood, et al., 2019; Wara et al., 2005) leading to an "El Niño-like" mean state, although the magnitude of this

change is still debated (Meinicke et al., 2021; Tierney, Haywood, et al., 2019). Meridional temperature gradients were also reduced (Brierley et al., 2009; Fedorov et al., 2015; Tierney, Haywood, et al., 2019), associated with changes in the distribution of subtropical rainfall (N. J. Burls & Fedorov, 2017) and ocean circulation in the Pacific (N. J. Burls et al., 2017; Ford et al., 2022). Upwelling zones along the eastern boundaries of the major ocean basins were substantially warmer (3°C–9°C) (Dekens et al., 2007) leading to shifts in the regional hydrological cycle (Bhattacharya et al., 2022; Fu et al., 2022; Rubbelke et al., 2023). In short, the Pliocene represents a major reorganization of the climate system at CO_2 concentrations similar to or lower than (ca. 370 ppm) (De La Vega et al., 2020) present-day values. Elucidating the patterns of climate change during this warm climate interval will improve our view of how the Earth's climate will behave in the future.

Here, we use paleoclimate data assimilation to produce spatial reconstructions of Pliocene climate. Paleoclimate data assimilation blends information from climate model simulations and proxy data, resulting in data-informed, dynamically consistent estimates of past climate states (Hakim et al., 2016; Osman et al., 2021; Tierney et al., 2020). We assimilate proxy estimates of SST with model simulation output from the PlioMIP2 (Haywood et al., 2020) and "Pliocene-like" simulations with altered cloud distributions (N. Burls & Fedorov, 2014; Erfani & Burls, 2019; Ford et al., 2022) to produce reconstructions for two time windows: the mid-Pliocene (3.5–3.0 Ma) and the early Pliocene (5.0–4.5 Ma). The mid-Pliocene reconstruction serves as a point of comparison for the numerous proxy and modeling-based syntheses targeting this particular time period (Haywood et al., 2020; McClymont et al., 2020), whereas the early Pliocene reconstruction addresses past observations suggesting it is even warmer than the mid-Pliocene, with very different zonal and meridional SST gradients (Fedorov et al., 2013). In addition, the upcoming PlioMIP3 project explicitly targets the early Pliocene (Haywood et al., 2024). Since it is spatially complete, "plioDA" provides an updated estimate of GMST for each of these time intervals, as well as equilibrium climate sensitivity (ECS). plioDA also yields new constraints on the patterns of SST change and provides inferred precipitation, evaporation and SSS fields, with implications for the hydrological cycle as well as ocean circulation.

2. Materials and Methods

2.1. Sea-Surface Temperature Proxy Data

We compiled three types of SST proxies: (a) the unsaturation ratio of C_{37} ketones (alkenones; $U^{K'}_{37}$), (b) the tetraether index of 86 carbons (TEX_{86}), and (c) the magnesium-to-calcium ratio of planktic foraminifera (Mg/Ca). U^{K}_{37} and TEX_{86} are based on the relative abundances of the molecular lipid fossils of haptophyte algae and pelagic Thaumarchaeota, respectively. In both cases, the microorganisms change the structure of their lipids in response to water temperature; for U^{K}_{37}, algae produce alkenones with fewer unsaturations at higher SST (Brassell et al., 1986), and for TEX_{86}, archaea produce tetraethers with more rings at higher SST (Schouten et al., 2002). The Mg/Ca proxy is based on the concentration of Mg measured in the calcium carbonate shells of foraminifera living in the mixed layer. More Mg is incorporated into the shells at higher SST (Cronblad & Malmgren, 1981). However, Mg/Ca in foraminiferal shells can also be affected by salinity and changes in the ocean carbonate system (Gray & Evans, 2019), which we address in the proxy system models used in the data assimilation (see Section 2.3 below). Pliocene SST inferences based on assemblages of foraminifera and diatoms also exist (Dowsett et al., 1996, 2010); however, proxy system models for these faunal methods that we can incorporate into the data assimilation framework have not yet been developed. In addition, some of these data are qualitative.

Previous Pliocene synthesis work has focused on Pliocene climate during a specific interglacial within the Piacenzian stage (KM5c, 3.205 ±0.01 Ma, McClymont et al. (2020)) so as to better compare with our current interglacial period. However, using this narrow temporal window substantially limits the number and spatial distribution of proxy records that can be included in our reconstruction. In order to include as many proxies as possible, we chose a wider (0.5 Ma) window for each of our target timeslices. Proxy values from each site were averaged across each target Pliocene timeslice (mid-Pliocene, 3.5–3 Ma; early Pliocene, 5.0–4.5 Ma), and these average values are used in the data assimilation. These windows span multiple glacial-interglacial cycles, meaning that our results represent long-term conditions as opposed to interglacial states. To investigate whether this choice biases our results (presumably toward cooler mean conditions in comparison to KM5c, since our window includes glacial states) we conducted a data assimilation experiment for the mid-Pliocene using only data securely dated to KM5c to compare with our result using the wider window.
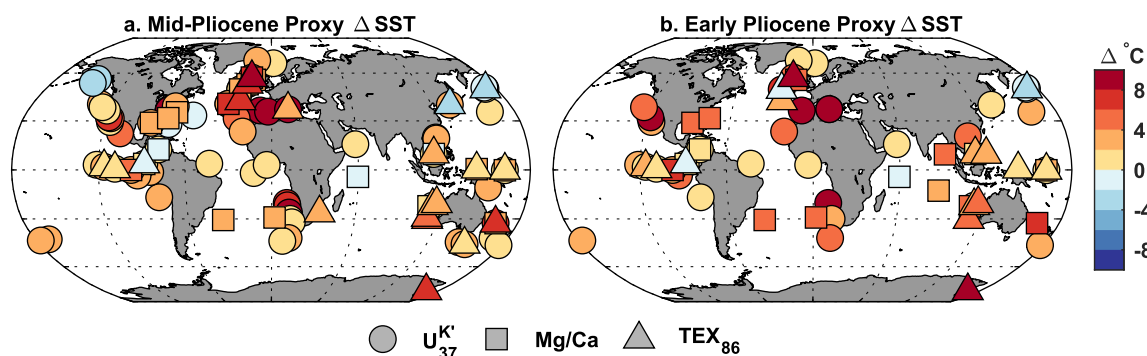
Figure 1. Sea-surface temperature (SST) proxy data used in the PlioDA reconstruction. Computed proxy SST anomalies for (a) the mid-Pliocene ($N = 108$) and (b) early Pliocene ($N = 64$), relative to preindustrial conditions.

During the compilation process, we screened the records and removed data from sites where non-thermal impacts on the proxy signature were suspected, either on the basis of the interpretations of the original authors, or due to physically unrealistic proxy signatures. A list of excluded proxy records and the rationale for exclusion is given in Table S2. For TEX_{86} data, we flagged points that may be impacted by the contribution of GDGTs by non-pelagic Thaumarchaeota using the Branched and Isoprenoid Tetraether index and Methane Index where these metrics were available (see Notes column in Table S1). These points were then excluded from site averages used for the data assimilation.

After compilation and screening, the SST proxy data used in this reconstruction consist of 116 published records from 88 unique sites, with 108 and 64 proxy entries available for the mid-Pliocene and early Pliocene timeslices, respectively (Figure 1; Table S1). Of the three proxies, U_{37}^{K} data are the most abundant, accounting for 63% of the data in the mid-Pliocene and 53% of the data in the early Pliocene. If we filter the mid-Pliocene proxies to only isolate sites with well-dated and resolved KM5c data, the dataset is reduced to 49 records from 39 unique sites.

Since we aim to analyze Pliocene climate relative to preindustrial conditions, each proxy site and type requires a preindustrial estimate. To assign a preindustrial proxy value, we followed the same approach as Tierney, Haywood, et al. (2019). Briefly: whenever possible, we used a late Holocene measurement on the same core or from a nearby (< 300 km) coretop. In cases where there were no nearby coretop data, we forward-modeled a proxy value using the 1870–1900 AD average SST from the HadISST1 reconstruction (Rayner et al., 2003). The method of preindustrial inference is provided in Table S1. Although the data assimilation takes place in native proxy units (see Section 2.3), Figure 1a and *b* show the computed proxy SST anomalies (mid-Pliocene − preindustrial, early Pliocene − preindustrial) for reference, using the inverse versions of the SST forward models described in Section 2.3.

Over the past 5 Myr, the locations of the proxy sites have shifted slightly due to plate tectonics. Although in most cases the change is minimal, there are exceptions. For example, Site ODP 1241 (5.8°N, 86.4°W) sits on the Cocos Plate, which has migrated northeast over the past few million years such that this site was located at 2.8°N, 89.2°W during the early Pliocene. Since these movements affect the SST signature recorded by the proxies, we calculated locations for each of our proxy sites at 3.25 Ma and 4.75 Ma using the plate rotation reconstruction of Müller et al. (2019) and GPlates version 2.3 (Müller et al., 2018). The proxy data are then assimilated at their appropriate paleolocations for each of our Pliocene timeslices.

2.2. Model Simulations

Our reconstruction uses model output from 14 PlioMIP2 simulations (Haywood et al., 2020; Chandan & Peltier, 2017; Hunter et al., 2019; Q. Zhang et al., 2021; Chan & Abe-Ouchi, 2020; Tan et al., 2020; Li et al., 2020; Feng et al., 2020; Lurton et al., 2020; Williams et al., 2021), two additional Pliocene sensitivity simulations with the CESM version 2 (Feng et al., 2022), and 21 "Pliocene-like" experiments with CESM version 1 with altered cloud albedo or low cloud fraction (hereafter referred to as the "cloud" simulations) (N. Burls & Fedorov, 2014; Erfani & Burls, 2019; Ford et al., 2022).

The PlioMIP2 simulations set CO_2 concentrations at 400 ppm and used the PRISM4 boundary conditions (Dowsett et al., 2016) which include changes in land/sea distribution, topography and bathymetry, land ice, soils, vegetation, and lakes. Most notably, these include large reductions in the Greenland and west Antarctic ice sheets, the closure of the Bering Strait, and greening of the Sahara and high latitudes. Three of the PlioMIP2 simulations were not included, two because monthly SST and SSS fields were not available at the time of analysis (the CCSM4-Utrecht (Baatsen et al., 2022) and MRI-CGCM simulations). A third model, the COSMOS simulation, Stepanek et al. (2020) was excluded because initial testing indicated that it introduced spatial artifacts into the prior and posterior due to the low resolution and type of grid used for the ocean component model ($3.0° \times 1.8°$, bipolar orthogonal curvilinear grid). The additional CESM2 experiments include one experiment with Pliocene CO_2 (400 ppm) but preindustrial boundary conditions, and another with Pliocene CO_2, topography, and bathymetry, but preindustrial ice and vegetation (Feng et al., 2022).

The cloud simulations were designed to test the impact of cloud distributions on zonal and meridional temperature gradients and mimic the reduced gradients observed in the Pliocene (N. Burls & Fedorov, 2014; Erfani & Burls, 2019; Ford et al., 2022). The simulations of N. Burls and Fedorov (2014) were conducted under preindustrial boundary conditions (CO_2 = 285 ppm, modern topography and bathymetry). The simulations of Erfani and Burls (2019) were conducted with modern topography and bathymetry but include experiments run under both preindustrial and $2 \times CO_2$ levels. The early Pliocene-like simulation of Ford et al. (2022) used preindustrial boundary conditions, while the mid-Pliocene-like simulation used preindustrial topography and bathymetry but a CO_2 concentration of 400 ppm. The cloud simulations produce a wide range of absolute GMST values (6°C–23°C), some of which are physically unrealistic for the Pliocene state (e.g., 6° would be a temperature typical of a Pleistocene glacial, while 23°C would be a temperature akin to the ice-free late Eocene). We therefore only included experiments where the change in GMST (ΔGMST) relative to the preindustrial simulation was between 1 and 8°C.

Table S3 provides a complete list and description of the model experiments. From each experiment, we used the average climatology from the last 100 years of the simulation as a prior state for the data assimilation (hereafter called the "prior"), so that each model experiment is represented once per target timeslice. Since the data assimilation method requires that the model output be on a consistent grid, we regridded all of the fields used in the reconstruction to $1° \times 1°$ resolution prior to assimilation. All of the Pliocene or Pliocene-like experiments have a corresponding preindustrial control experiment, and these simulations were used as the prior for our preindustrial timeslice. The same set of Pliocene and Pliocene-like simulations was used as the prior for both the mid-Pliocene and early Pliocene timeslices. However, since the PlioMIP and cloud simulations differ in their boundary conditions, we also conducted PlioMIP-only and cloud-only assimilation experiments to compare with our main results, which use the full set of simulations.

In all, the multi-model prior ensemble includes 37 members for the Pliocene time slices and 17 members for the preindustrial slice. Figure 2 shows the multi-model Pliocene prior mean for surface air temperature (SAT, Figure 2a), SST (Figure 2b), and GMST (Figure 2c), relative to the preindustrial simulations. We also show the model range in the Pliocene–preindustrial tropical Pacific zonal gradient (Figure 2d). Following Tierney, Haywood, et al. (2019), this gradient is computed as the difference between the average SST of the western Pacific warm pool (WPWP; 10°S–10°N, 130–170°E) and the eastern equatorial Pacific (EEP; 2°S–2°N, 90–140°W). The span in GMST and the Pacific zonal gradient (Figure 2) illustrates that the range of potential Pliocene climate states represented by our model prior is large, which ensures that the posterior is not constrained by a lack of variability or individual model physics (Annan et al., 2022).

2.3. Paleoclimate Data Assimilation

Following previous paleoclimate data assimilation work (Osman et al., 2021; Tierney et al., 2020, 2022) we use an offline ensemble Kalman filter method to assimilate the SST proxy data with the model prior ensemble, using the Matlab toolbox DASH v. 4.2.2 (King et al., 2023). We refer the reader to these previous works for a full description of the mathematics and the code. Briefly, the method produces a posterior climate state (X_{post}) from the linear combination of the model prior (X_{prior}) and the proxies (Y):

$$X_{post} = X_{prior} + K(Y - Y_e) \tag{1}$$
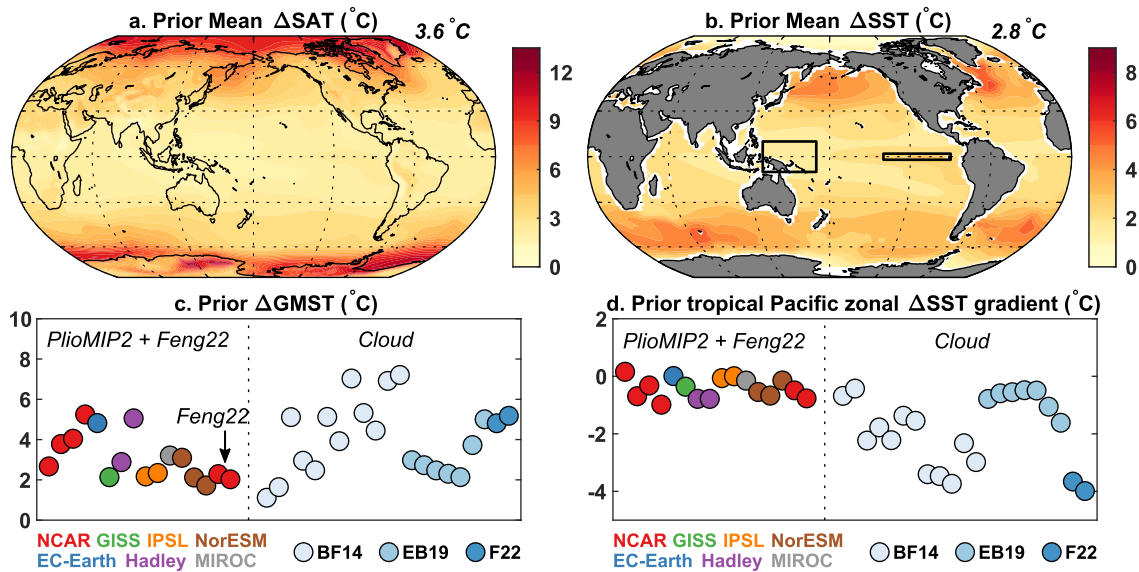
Figure 2. Overview of the model prior ensemble. Each panel shows the Pliocene−preindustrial difference. Spatial pattern of the prior mean change in (a) surface air temperature and (b) sea-surface temperature (SST), with global mean changes shown in the upper right hand corner; Prior change in (c) global mean surface temperature and (d) The tropical Pacific zonal gradient for each Pliocene ensemble member ($N = 37$). The zonal gradient is calculated as the average difference between mean SST in the western Pacific warm pool (10°S–10°N, 130–170°E) and the eastern equatorial Pacific cold tongue (2°S–2°N, 90–140°W); boxes corresponding to these regions are shown in panel (b) The pliocene modeling intercomparison project phase 2 and Feng22 modeling experiments are colored by model family. In panel c, the arrow points to the Feng22 experiments (Feng et al., 2022) for clarity. The altered cloud runs are shown in light blue shades; BF14 = N. Burls and Fedorov (2014), EB19 = Erfani and Burls (2019), F22 = Ford et al. (2022).

where K represents the Kalman gain:

$$K = cov(X_{prior}, Y_e) \times [cov(Y_e, Y_e) + R]^{-1} \qquad (2)$$

X_{prior} is a $N \times M$ matrix of the model simulation output (Section 2.2), where N consists of all of the model fields to be updated (monthly and mean annual values for SST, SSS, SAT, precipitation, and evaporation) collapsed into a state vector, and M is the number of ensemble members. Y is the proxy information (Section 2.1) of dimension $P \times M$, where P is the number of proxies available for each target timeslice, tiled M times to form a matrix compatible with the update equation. Y_e is the model estimate of the proxy value, also of dimension $P \times M$. The difference between the observed proxy values Y and model-predicted values Y_e is called the "innovation" and represents the new information coming from the proxy data. This term is added to X_{prior} weighted by K, the Kalman gain. The first term of the Kalman gain, $cov(X_{prior}, Y_e)$, describes the relationship between the model prior and the model-predicted proxy values, and effectively "spreads" the proxy update across the prior state. The second term, $[cov(Y_e, Y_e) + R]^{-1}$, represents the errors, including the covariance of the proxy estimates Y_e and the observed proxy covariance (R). R is a diagonal matrix, that is, the errors associated with each proxy are assumed to be independent from one another.

To compute Y_e, we take the model output from X_{prior} at the location of the proxies and forward-model it into proxy values of $U^{K'}_{37}$, Mg/Ca, and TEX$_{86}$ using the Bayesian proxy models BAYSPLINE (Tierney & Tingley, 2018), BAYMAG (Tierney, Malevich, et al., 2019), and BAYSPAR (Tierney & Tingley, 2014) (in "standard" mode, as opposed to "analogue" mode), respectively. Forward modeling of $U^{K'}_{37}$ and TEX$_{86}$ is straightforward and only requires SST from the model output. The Mg/Ca proxy requires constraints on surface ocean pH, calcite saturation state (Ω) at the water depth of the core site, SSS, the Mg/Ca composition of the seawater (Mg/Ca$_{sw}$), and the laboratory cleaning method. The latter information is available from the original studies and SSS is available from the model output. For pH and Ω, we use modern values for all of the target timeslices from the GLODAPv2 gridded dataset (Lauvset et al., 2016). Since Pliocene CO_2 concentrations were similar to modern day, this is a reasonable assumption for pH, although there were very likely regional changes in response to shifts in ocean circulation (Shankle et al., 2021). Likewise, deep ocean saturation state may be somewhat different than present-

day (N. J. Burls et al., 2017), but in the absence of global reconstructions of the Pliocene ocean carbonate system, holding these values at modern levels is a prudent choice. Unless Ω drops to values lower than 0.9, the impact of this choice would affect Mg/Ca-derived SST estimates by less than a degree.

We estimate past Mg/Ca_{sw} using BAYMAG with two additional updates. First, we update the Mg/Ca_{sw} reconstruction in BAYMAG to include newer Na/Ca-based Mg/Ca_{sw} estimates (Rosenthal et al., 2022; Zhou et al., 2021) and exclude the coral Mg/Ca_{sw} inferences (Gothmann et al., 2015) from the last 20 Ma, which have large uncertainties. This revised Mg/Ca_{sw} reconstruction shows a larger change in Mg/Ca_{sw} over the past 15 Ma than the original BAYMAG reconstruction, indicating a Mg/Ca_{sw} of 4.4 and 4.1 for our target timeslices of 3.25 Ma and 4.75 Ma respectively (Figure S1 in Supporting Information S1). Second, we incorporate a non-linear power component (H) into the Mg/Ca_{sw} - Mg/Ca_{foram} relationship into the BAYMAG model following geochemical expectations (Evans & Müller, 2012). Based on a synthesis of culture and inorganic precipitation experiments, we use an H of 0.74 in our forward model application for all species (Text S1 in Supporting Information S1, Figure S2 in Supporting Information S1).

R (Equation 2) is user-defined and should ideally represent all of the uncertainties surrounding the proxy observation (analytical and environmental). The Bayesian forward models provide a relatively conservative estimate of R associated with the calibration data sets used to train the models. We tested whether scaling R to a lower value would improve internal proxy validation (Text S2 in Supporting Information S1) but found little evidence of an improvement in skill, so we use the forward model values of R unscaled. These variances are 0.0025 for $U_{37}^{K'}$ and TEX_{86} and 0.0169 for Mg/Ca (in natural log units), which roughly correspond to 1.5°C, 3.5°C, and a 2.2°C 1σ uncertainties, respectively.

In addition to the specification of R, another user-defined choice in data assimilation is covariance localization, which limits how far a proxy can update the prior state in space. Localization is a distance-weighted filter that is multiplied with each of the two terms in the Kalman gain (Equation 2). Beyond a specified cut-off radius, the model prior is not updated, therefore limiting spurious far-field updates. However, if the localization radius is too small, meaningful teleconnections might be excluded. Based on both internal and external validation tests (Text S2 in Supporting Information S1, Figures S3 and S4 in Supporting Information S1) we determined that a localization radius of 24,000 km was the most appropriate choice for our reconstructions.

Results shown in the main text include all model simulations in the prior. However, we also conducted DA experiments that use only the PlioMIP2 simulations ($N = 14$) or the cloud simulations ($N = 21$), respectively, to assess the sensitivity of the results to the different types of model priors.

3. Results

The mid-Pliocene and early Pliocene reconstructions from plioDA show a similar pattern of SST change (Figures 3a and 3b) that is amplified during the earlier period. The largest SST changes occur in the North Atlantic and Indian Ocean sector of the Southern Ocean. Both the Atlantic and Pacific oceans show more warming in the eastern boundary current regions, and there is also enhanced warming in the EEP relative to the WPWP. These general features of the SST pattern emerge regardless of whether the entire prior is used or if only PlioMIP2 and cloud simulations are used, respectively (Figure S5 in Supporting Information S1). They are also apparent in our KM5c-only sensitivity experiment (Figure S6 in Supporting Information S1) with a slightly reduced magnitude. In the North Pacific, the mid-Pliocene plioDA reconstructs a unique pattern consisting of elevated warmth along the southern boundary of the North Pacific subtropical gyre and in the Kuroshio extension area, coupled with muted warming in the Gulf of Alaska (Figure 3a). This pattern is also seen in the PlioMIP2-only DA experiment, but not in the cloud-only DA experiment (Figure S5 in Supporting Information S1). It appears in the KM5c-only mid-Pliocene experiment, but is weakly expressed (Figure S6 in Supporting Information S1).

The posterior SAT fields show amplified warming in the high latitudes (Figures 3c and 3d) with the largest change occurring in regions that experienced substantial ice loss (e.g., over Greenland, where most of the present-day ice sheet was exposed land during the Pliocene). When the changes in SAT are averaged across the globe, plioDA indicates that mid-Pliocene GMST was 4.1°C (95% CI = 3.0°C–5.3°C) warmer than preindustrial conditions, and that the early Pliocene was 4.8°C (95% CI = 3.6°C–6.2°C) warmer than preindustrial. The PlioMIP2-only and cloud-only experiments yield similar values for the change in GMST (Table S4 in Supporting Information S1).
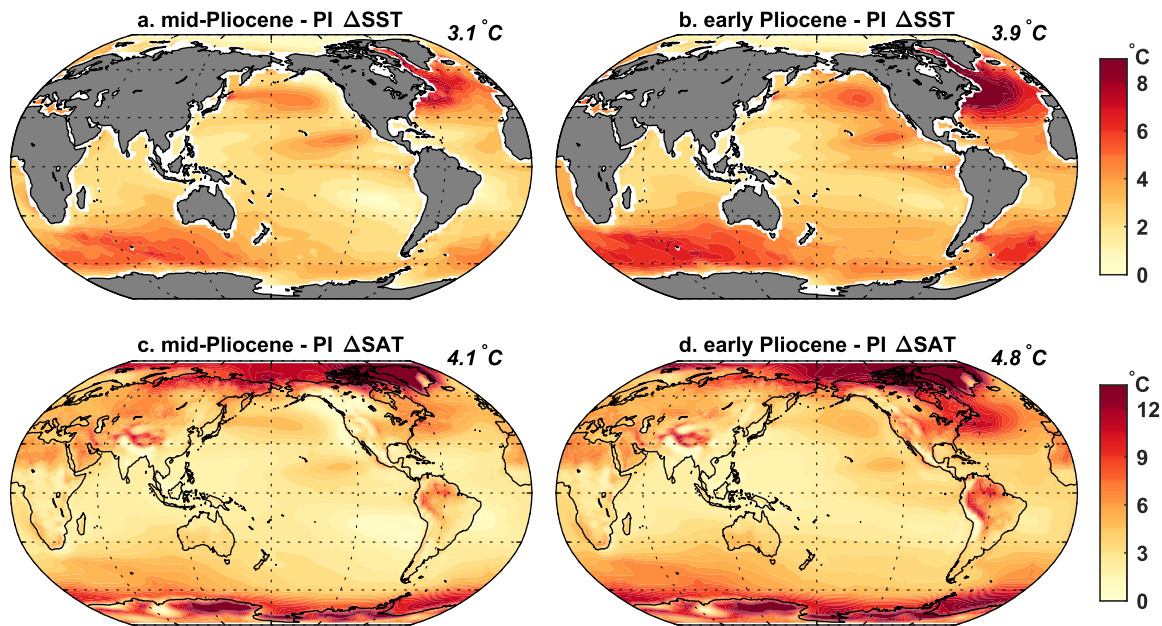
Figure 3. PlioDA mean annual temperature anomalies, relative to the preindustrial DA solutions. Average global mean temperature changes are shown in the upper right hand corner of each subplot. (a) mid-Pliocene change in sea-surface temperature (SST) (ΔSST). (b) early Pliocene change in SST (ΔSST). (c) mid-Pliocene change in surface air temperature (SAT) (ΔSAT). (d) early Pliocene change in SAT (ΔSAT).

The KM5c-only DA experiment yields a change in GMST that is indistinguishable from the main mid-Pliocene result (3.9°C, 95% CI = 2.6°C–5.4°C; Figure S6 in Supporting Information S1).

Assimilation of proxy SST data also allows us to recover posterior fields for variables that reflect the water cycle, since SST changes are related to hydrological patterns (Figure 4). While plioDA-inferred changes in mean annual Precipitation − Evaporation ($P - E$) show that the high latitudes uniformly get wetter during the mid-Pliocene, there are strong meridional differences in both the tropics and subtropics. In the tropics, the Afro-Asian monsoon domain and the region under the northern edge of the Pacific intertropical convergence zone (ITCZ) are wetter, while central America and tropical South America show severe drying. In the subtropics, the North Atlantic region is dry, while the eastern subtropical North Pacific is wet (Figure 4a). The PlioMIP2-only DA experiment results in similar reconstructed $P - E$ patterns as the full model prior, but the cloud-only DA experiment differs in many regions, exhibiting more of a general southwards shift of the ITCZ and a weaker African monsoon (Figure S7 in Supporting Information S1).
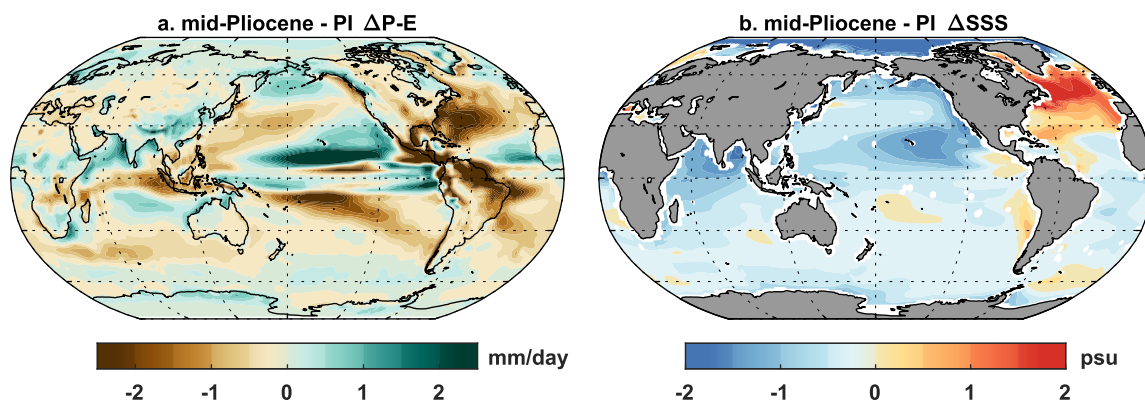
Figure 4. PlioDA mean annual anomalies in metrics of hydroclimate, relative to the preindustrial DA solutions (PI). (a) mid-Pliocene change in Precipitation − Evaporation (ΔP-E). (b) mid-Pliocene change in sea-surface salinity (ΔSSS).

mid-Pliocene SSS mirrors the large-scale changes in $P - E$, with the Indian Ocean and North Pacific becoming fresher relative to preindustrial conditions, and the North Atlantic saltier (Figure 4b). The PlioMIP2-only DA experiment is similar but shows more freshening in the Indian Ocean and a less salty North Atlantic (Figure S7 in Supporting Information S1). The cloud-only DA experiment shows a salty Atlantic and fresh Pacific but lacks the strong increase in salinity in the North Atlantic (Figure S7 in Supporting Information S1).

The early Pliocene changes in $P - E$ and SSS are very similar to the mid-Pliocene patterns (Figure S8 in Supporting Information S1), so in the discussion below we focus on the mid-Pliocene changes.

4. Discussion

4.1. Sea-Surface Temperature Patterns

The addition of the proxy data (Figure 1) to the model prior (Figure 2) has a noticeable effect on reconstructed patterns of SST change during the Pliocene. For example, the proxy data indicate enhanced warming in the North Atlantic (Figure 1), which clearly emerges in the posterior (Figures 3a and 3b). Strong warming in the North Atlantic is an expected consequence of the closure of the Bering Strait and Canadian Arctic Archipelago Straits, which reduces freshwater export from the Pacific to the Atlantic and strengthens Atlantic Meridional Overturning Circulation (AMOC) (Brierley & Fedorov, 2016; Otto-Bliesner et al., 2017; Weiffenbach et al., 2023). However, it is not clear whether the straits were open or closed during the Pliocene, since some geological evidence suggests the Bering Strait opened during the late Miocene (Hall et al., 2023; Marincovich et al., 1999). The PlioMIP2 simulations have these straits closed, but the cloud simulations do not (since they were conducted under modern boundary conditions) hence both configurations are present in the prior. The DA posterior shows strong warming in the North Atlantic even when only the cloud simulations (straits open) are used as the prior (Figure S5 in Supporting Information S1), suggesting that a warm North Atlantic emerges from assimilation of the data regardless of the imposed boundary conditions. This nominally supports closure of the Arctic gateways during the Pliocene, although, we cannot rule out the possibility that this region was warm for another reason, such as changes in atmospheric stationary waves caused by a smaller Greenland ice sheet and vegetation changes over the northern high latitudes. Regardless of the exact cause, the fact that the posterior using the full prior is very similar to the posterior using PlioMIP2 simulations only (Figure S5 in Supporting Information S1) suggests that the PlioMIP2 boundary conditions (in the North Atlantic and elsewhere) are highly compatible with the SST proxy data. We also note that our KM5c-only DA experiment shows a warm North Atlantic as well, although the anomaly is slightly reduced in magnitude since fewer proxy data sites participate (Figure S6b in Supporting Information S1), indicating that this is a robust feature of the Pliocene mean state.

The assimilation of the proxies also alters the warming patterns in the Pacific ocean. Whereas the model prior mean shows warming of ca. 4.5°C uniformly across the North Pacific subpolar gyre (Figure 2b), the plioDA mid-Pliocene posterior focuses this warming into the Kuroshio extension region and reconstructs almost no warming in the Gulf of Alaska (Figure 3a). This reflects both alkenone and TEX$_{86}$ data that show a lack of warming (or even a slight cooling) in the Gulf of Alaska and also in the subpolar North Pacific off of the Kamchatka Peninsula (Figure 1a). The result is that the North Pacific inherits a SST pattern similar to the negative phase of the Pacific Decadal Oscillation (PDO) (Mantua et al., 1997), in which the north-central Pacific ocean warms while the Gulf of Alaska cools.

Although the negative phase of the PDO is usually accompanied by La Niña-like conditions (Mantua et al., 1997), during the Pliocene the tropical Pacific was clearly El Niño-like (Tierney, Haywood, et al., 2019; Wara et al., 2005) (and see discussion below). In addition, proxies indicate that the California margin was very warm (see Figure 1) which also conflicts with a PDO negative pattern. This results in muted warming in this region in the posterior plioDA solution as it seeks to balance the proxy evidence within the constraints of model covariance (Figure 3a). The mid-Pliocene North Pacific SST pattern is therefore somewhat unusual; however, North Pacific ocean-atmosphere dynamics need not move in lockstep with the tropical Pacific as they are strongly influenced by oscillations in the Aleutian Low (Newman et al., 2016). Following the PDO analogy, the localized warming in the Kuroshio extension region would be consistent with a weaker Aleutian Low and a poleward shift in the westerly storm track, the latter of which dust flux reconstructions support (Abell et al., 2021). Notably, the North Pacific pattern is present in the PlioMIP2-only DA experiment, but not in the cloud-only experiment, where both the mid-latitude eastern North Pacific and the Gulf of Alaska are reconstructed to show minimal warming (Figure S5 in Supporting Information S1). This suggests that Pliocene boundary conditions (in particular, high latitude changes
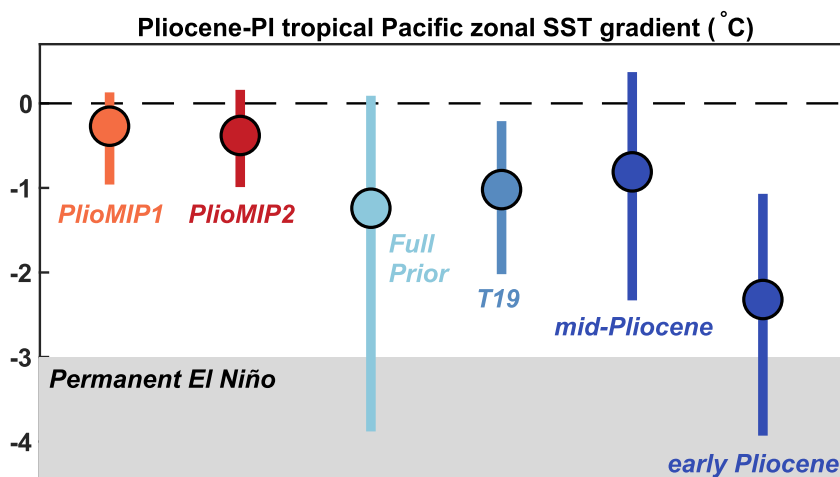
Figure 5. PlioDA reconstructed change in the tropical Pacific gradient for both the mid- and early Pliocene (dark blue), compared to model simulations and a previous proxy-based inference. Dots indicate mean values, error bars show the 95% confidence interval. PlioMIP1 (orange) excludes the COSMOS and MRI experiments, which simulate an unrealistic increase in the zonal gradient. Pliocene modeling intercomparison project phase 2 (PlioMIP2) (red) summarizes the simulations used in our model prior (i.e., excludes COSMOS, MRI, and CCSM4-Utrecht). The full model prior (light blue) includes both PlioMIP2 and the cloud simulations. T19 is the mid-Pliocene alkenone-based estimate from (Tierney, Haywood, et al., 2019). The shading below −3°C indicates "permanent El Niño" conditions.

in land ice and vegetation) may play a role in shaping this unusual pattern. Further SST proxy investigations, particularly in the central North Pacific where currently there are no data, will provide a critical test of whether the North Pacific SST pattern in plioDA is robust.

The North Pacific warming pattern is evident in the KM5c-only experiment (Figure S6b in Supporting Information S1) but it is poorly defined because only two sites in the North Pacific contain KM5c data. Restricting the time window for the mid-Pliocene to the KM5c interglacial also eliminates all of the data from the California margin, such that the robust warming of this region evident in the data (Dekens et al., 2007) does not enter into the DA. Our expanded mid-Pliocene time window of 3.5–3 Ma therefore is justified since it is needed to capture this important feature of Pliocene Pacific climate change.

The Gulf of Alaska sites (ODP 887 and IODP 1417) do not have data during the early Pliocene (Figure 1b), so for this timeslice, the warming in the Kuroshio extension expands into the Gulf of Alaska (Figure 3b). However, the general SST pattern in the North Pacific remains similar, with three loci of warming in the Kuroshio extension, off of Baja California, and in the EEP. Without the muted warming in the Gulf of Alaska, the magnitude of California margin SST change (6°C) for the early Pliocene is in better agreement with the proxy evidence (Dekens et al., 2007), but the epicenter of warming is still located further offshore than the proxy locations. The resolution of the ocean models used in plioDA (typically 1°; Table S3) limits its ability to capture warming in coastal upwelling regions. In addition, non-overlapping ocean grids across the multi-model prior result in missing grid cells along the coastlines. Hence, it is possible that coastal upwelling zones were warmer than plioDA shows, a feature that is critical for altering the seasonal hydrological cycle during the Pliocene (Bhattacharya et al., 2022; Rubbelke et al., 2023).

The EEP and the WPWP are relatively well-sampled by proxy data (Figure 1) and changes in the tropical Pacific zonal gradient in the model prior are broad by design (Figures 2d and 5) allowing plioDA to provide the best possible multi-proxy, multi-model reconstruction of this key feature of Pliocene tropical climate. For the mid-Pliocene timeslice, plioDA indicates a mean change in the Pacific zonal gradient (calculated in the same manner as for the model prior, see Section 2.2) of −0.8°C (95% CI = −2.3°C–0.4°C), which is slightly smaller than the prior mean (−1.2°C). This result is similar to the alkenone-only reconstruction of Tierney, Haywood, et al. (2019), which indicates −1.0°C change across the 3–3.5 Ma time period (Figure 5), as well as TEX$_{86}$-based reconstructions (Y. G. Zhang et al., 2014; O'Brien et al., 2014). However, we consider the plioDA result more robust because, unlike this previous work, it is informed by three different types of proxies, leverages all data with covariance relationships to the tropical Pacific, and does not rely on the use of historical El Niño and La Niña

warming patterns. The plioDA mean change is lower than the PlioMIP multi-model means, which are relatively consistent between PlioMIP1 and 2 (−0.3 and −0.4°C, respectively; Figure 5). If we only use PlioMIP2 simulations in the model prior, the posterior mean change in the Pacific zonal gradient increases to −0.4°C (Table S4 in Supporting Information S1), as the limited range of change in PlioMIP2 constrains the reconstruction. Conversely, if we only use the cloud simulations, we get a similar result as the full prior (posterior mean of −1.1°C; Table S4 in Supporting Information S1). This underscores the importance of including the cloud simulations in order to create a wide enough prior for the Pacific zonal gradient. It also suggests that, while some individual models within PlioMIP2 can simulate a zonal gradient reduction similar to that of the proxies, many underestimate the change.

Although it is unlikely (<10% probability), plioDA does not rule out no change (or even a slight increase) in the Pacific zonal gradient during the mid-Pliocene. However, in the cloud-only DA experiment, this possibility is eliminated (the 95% CI becomes −2.1−−0.4°C; Table S4 in Supporting Information S1), which suggests this result is not an inherent feature of the data but more likely reflects the prior. The PlioMIP2 ensemble includes one simulation with an increase in the Pacific zonal gradient (CCSM4-NCAR), and two with a near-zero change (EC-Earth3 and IPSL-CM5A) so the lingering probability of no change or an increase in the zonal gradient likely reflects the projection of these prior ensemble members onto the posterior.

Following Tierney, Haywood, et al. (2019), we consider a so-called "permanent El Niño" condition to be a Pacific zonal gradient change of −3°C (relative to preindustrial) or less, which corresponds to an absolute west-east gradient of 1.2°C, the average value across four of the largest historical El Niño events (1877, 1982, 1997, 2015). The plioDA mid-Pliocene timeslice mean is far away from this condition, and does not overlap it within posterior uncertainty (Figure 5). This is also the case for the cloud-only DA experiment (Table S4 in Supporting Information S1). The original "permanent El Niño" study of Wara et al. (2005) reconstructed a Pacific zonal gradient close to zero (an anomaly of −4°C, equivalent to an absolute west-east gradient of 0.2°C) during the mid-Pliocene; however, this was an overestimate because the changing composition of Mg/Ca of seawater was not considered. With the latest Mg/Ca_{sw} reconstruction of Rosenthal et al. (2022), which we use here in plioDA, the Mg/Ca data from Wara et al. (2005) (sites ODP 806 and ODP 847) indicate −2.8°C of change—still very large, but more physically plausible because the WPWP remains warmer than the EEP. This information is incorporated into plioDA, but, it is balanced by other proxies at different locations in the WPWP and EEP. Given that the inferred zonal gradient change from these two sites alone lies outside of the 95% CI of the plioDA posterior for the mid-Pliocene, it suggests that these data are not representative of the regional average. This underlines the strength of a spatial reconstruction approach like paleoclimate data assimilation, which leverages all of the available proxy information and their covariance with one another.

In contrast with the mid-Pliocene timeslice, the early Pliocene plioDA reconstruction indicates an average gradient change of −2.3°C (95% CI = −3.9−−1.1°C) and its uncertainty range overlaps with "permanent El Niño" conditions (Figure 5). With the cloud-only prior, the mean Pacific zonal gradient change decreases further to −2.7°C (Table S4 in Supporting Information S1). The large warming in the EEP of ca. 4°C is visually apparent in the map of the posterior SST results (Figure 3b). The zonal gradient change lies well outside the reductions simulated by the PlioMIP experiments, which indicates that the tropical Pacific was in a much different state at 4.75 Ma versus 3.25 Ma and that this is not well-captured by standard mid-Pliocene simulations. One possible difference between the two time periods is the Isthmus of Panama, which some reconstructions suggest was not fully developed until the mid-Pliocene (O'Dea et al., 2016). However, more recent plate reconstructions as well as geological data suggest that the isthmus was present since the Miocene, although shallow connections between the Pacific and Atlantic could have existed through the Pliocene (McGirr et al., 2021; Vallejo-Hincapié et al., 2024). Moreover, model simulations suggest that removing the isthmus cools the EEP rather than warming it (Brierley & Fedorov, 2016). Another possible difference between the time periods is atmospheric CO_2 concentrations, but available CO_2 proxy data don't show an obvious difference (Guillermic et al., 2022; Sosdian et al., 2018; Tanner et al., 2020; De La; Vega et al., 2020). Our finding of a very different Pacific zonal gradient only 1.5 Ma before the mid-Pliocene warrants further study of the early Pliocene, as well as its proposed inclusion in the next Pliocene Modeling Intercomparison Project (PlioMIP3) (Haywood et al., 2024).
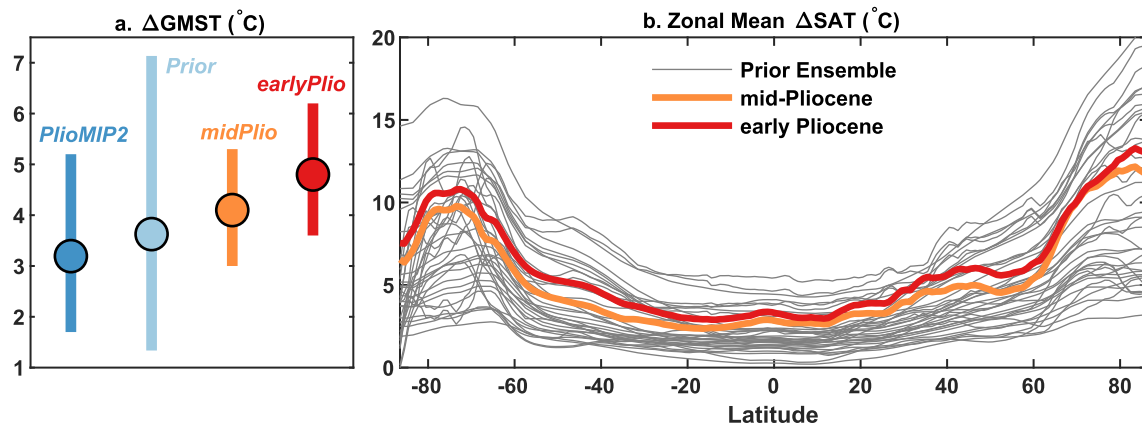
Figure 6. plioDA posterior global mean surface temperature (GMST) change and zonal mean surface air temperature (SAT) change compared to pliocene modeling intercomparison project phase 2 (PlioMIP2) and the model prior. (a) Change in GMST (ΔGMST) in the PlioMIP2 ensemble (dark blue), the model prior (light blue), the mid-Pliocene plioDA posterior (orange), and the early Pliocene plioDA posterior (red). Dots indicate the mean values and bars represent the 95% confidence intervals. (b) Zonal mean annual SAT change (ΔSAT) in the plioDA mid-Pliocene (orange) and early Pliocene (red) reconstructions. Zonal ΔSAT for individual prior ensemble members are plotted in gray.

4.2. Pliocene Warmth and Polar Amplification

The plioDA change in GMST for the mid-Pliocene (4.1°C warmer than preindustrial, on average, 95% CI = 3.0°C–5.3°C), is higher than the PlioMIP2 average (3.2°C) (Haywood et al., 2020) as well as the range given in the IPCC AR6 report (2.5°C–4.0°C, based on a scaling proxy global SST estimates to GMST; Gulev et al. (2021)). It is, however, within the spread of the PlioMIP2 model ensemble (Figures 2c and 6a). Although it is warmer than previous estimates, 4.1°C is a reasonable result given that alkenone proxy data from the KM5c interglacial suggest 3.0°C of ocean warming (McClymont et al., 2020) (which agrees well with the mid-Pliocene global SST change of 3.1° that we reconstruct here) and terrestrial proxies suggest amplified warming on land, particularly in the high latitudes (Salzmann et al., 2013). Our reconstructed GMST change also agrees well with the recent data assimilation reconstruction of Annan et al. (2024) (3.9°C, 95% CI = 1.7°C–6.1°C) that only uses the alkenone $U^{K'}_{37}$ proxy data, but is warmer than their reconstruction that uses all proxy data (3.0°C, 95% CI = 1.7°C–5.0°C). This may be due to several factors, since the proxy network, model prior, and methodology in Annan et al. (2024) are all different than what we use in plioDA. Annan et al. (2024) only use data assigned to KM5c (i.e., they apply the PlioVar criteria (McClymont et al., 2020);); however, our assimilation experiment with KM5c data produces a similar GMST change as our main result (3.9°C on average) so we do not think the proxy network alone is responsible for the difference. Rather, one major factor may be the treatment of the Mg/Ca proxy data, which in the Annan et al. (2024) study are converted to temperature using a mixture of different calibrations and have a tendency to predict a cooler GMST change (due to cool SST anomalies in the deep tropics). Here, we use the BAYMAG forward model to treat the Mg/Ca in a consistent way, and we also incorporate the latest reconstruction of Mg/Ca of seawater (Rosenthal et al., 2022), which increases the SST anomalies for the tropical Mg/Ca sites in particular. As is evident in Figure 1, there are a few Mg/Ca sites that show slightly cooler-than-preindustrial anomalies in the mid- and early Pliocene, but in many locations Mg/Ca indicates warming of a similar magnitude to $U^{K'}_{37}$ and/or TEX$_{86}$. This emphasizes the importance of correctly modeling the non-thermal influences on the Mg/Ca proxy, as has been discussed previously in the context of interpreting Pliocene data (McClymont et al., 2020, 2023).

Although the 95% confidence intervals for the mid-Pliocene and early Pliocene change in GMST (4.8°C on average) overlap (Figure 6a), comparison of the posterior distributions of absolute GMST from the two time periods indicates that they derive from significantly ($p < 0.01$) different populations (non-parametric two-sample Kolmogorov-Smirnov test). In other words, the early Pliocene mean GMST is significantly warmer (0.7°C) than the mid-Pliocene mean according to plioDA, a difference that must derive from the assimilation of the SST data (the model priors are identical for the mid and early Pliocene reconstructions). The substantially warmer early Pliocene raises the question again as to whether atmospheric CO$_2$ concentrations were higher than during the mid-

Pliocene, and/or if other mechanisms are needed to explain the warm climate during this time (Fedorov et al., 2013).

The mid- and early Pliocene show similar patterns of zonal mean SAT response, and the posterior solutions for each time slice fall roughly in the middle of the prior model ensemble spread (Figure 6b), indicating that as with GMST, the prior model range adequately encompasses the zonal mean SAT implied by the data. plioDA shows substantial polar amplification, with high latitude (60–90°N and S) warming of 9.0°C and 9.9°C relative to preindustrial during the middle and early Pliocene times, respectively (Figure 6b). When ratioed to the GMST changes according to Smith et al. (2019), this yields polar amplification factors of 2.2 and 2.1, respectively. These values are close to the PlioMIP2 mean value (2.3) (Haywood et al., 2020). The PlioMIP2 ensemble, however, has a large range of differences in polar amplification between the NH and Southern Hemisphere (SH), with some models indicating more polar amplification in the NH and others in the SH (Haywood et al., 2020). plioDA clarifies this aspect of Pliocene warmth, indicating slightly more polar amplification in the NH (2.4) than the SH (2.0) for the mid-Pliocene (with a similar pattern in the early Pliocene, i.e., 2.2 and 1.9).

Unlike projections of future warming, which show much larger polar amplification in the NH (Hahn et al., 2021), the Pliocene features relatively symmetric polar amplification in the NH and SH (Figure 6b). In modern warming scenarios, the Arctic region warms more than the Antarctic largely due to the extensive Antarctic ice sheet, which, since it will not equilibrate with high CO_2 on human timescales, is not altered in these simulations. The Antarctic ice sheet has higher albedo than the Arctic region but also has higher elevation, which weakens the positive lapse rate feedback in the Antarctic region (Goosse et al., 2018; Hahn et al., 2021). In contrast, the substantial loss of west Antarctic ice prescribed as part of the PlioMIP2 boundary conditions (Dowsett et al., 2016) reduces albedo at around 70°S and could potentially allow the lapse rate feedback to strengthen, amplifying the warming. Single-forcing experiments confirm that the Antarctic ice sheet changes are primarily responsible for polar amplification in the Pliocene SH (Lunt et al., 2012), but plioDA provides a specific, data-informed zonal mean temperature target, which future work could use to formally diagnose the contributions of forcings and feedbacks to Pliocene polar amplification.

4.3. Pliocene Climate Sensitivity

Past climates are critical for providing constraints on ECS, or rather, the response of GMST to a doubling of CO_2. In particular, paleoclimates provide key insight on the upper bound of ECS, which is not well constrained by historical observations (Sherwood et al., 2020). As a moderately warmer-than-today climate with similar paleogeography and a CO_2 concentration of ~ 400 ppm, the Pliocene is an excellent target for studying ECS.

To estimate an ECS value from the Pliocene that is comparable to present-day calculations, one must treat the different boundary conditions (vegetation, ice sheets, paleogeography) as radiative forcings (PALAEOSENS Project Members, 2012) and make assumptions about trace GHG concentrations. Sherwood et al. (2020) computed present-day ECS from the mid-Pliocene using the following description of the energy balance:

$$\Delta T = \frac{-\Delta F_{CO2}\left(1 + f_{CH4}\right)\left(1 + f_{ESS}\right)}{\frac{\lambda}{(1 + \zeta)}} \tag{3}$$

from which ECS (termed S) can be computed as:

$$S = -\Delta F_{CO2}/\lambda \tag{4}$$

ΔF_{CO2} is the radiative forcing associated with the change in CO_2, $1 + f_{CH4}$ is additional forcing due to trace GHGs (mainly methane). $1 + f_{ESS}$ is the inflation factor associated with the radiative impact of changes in boundary conditions (where ESS stands for Earth system sensitivity). $1 + \zeta$ accounts for the difference between the "true" ECS (i.e., a state at equilibrium with respects to short-term feedbacks) represented by paleoclimate states and the effective climate sensitivity (S) calculated from model simulations, which is based on regression of 150 years of a model run and therefore doesn't include slower adjustments, such as those associated with the deep ocean (Sherwood et al., 2020). For the sake of comparison, we use the same values for these parameters as Sherwood et al. (2020). mid-Pliocene CO_2 concentrations are assumed to be 375 ± 25 ppm (1σ), which is close to the updated estimate of De La Vega et al. (2020) of 367 ppm. f_{CH4} is 0.4 ± 0.1 (1σ), which assumes that methane
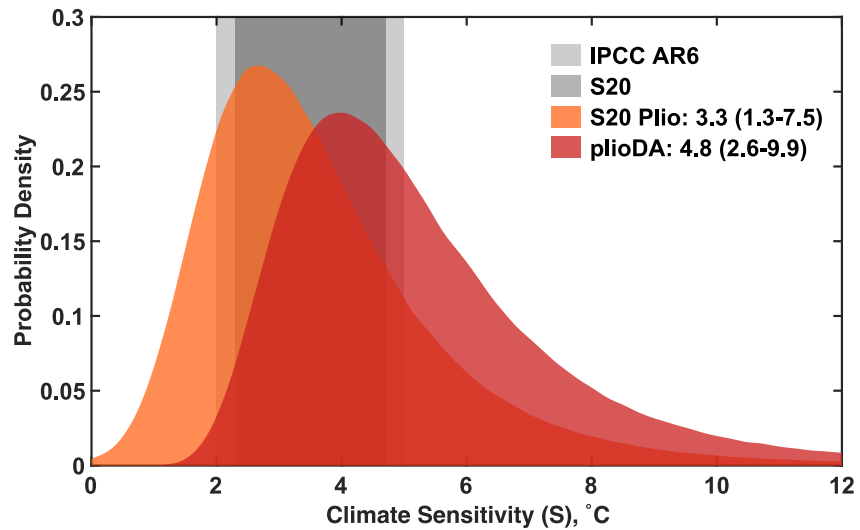
Figure 7. Climate sensitivity (*S*) estimated from the mid-Pliocene change in global mean surface temperature from plioDA (red) compared to the previous Pliocene estimate from Sherwood et al. (2020) (orange) and the 90% confidence intervals from the IPCC AR6 WG1 report (light gray) (Forster et al., 2021) and Sherwood et al. (2020) multiple lines of evidence posterior distribution (darker gray). The legend lists median values with 90% CI ranges in parentheses.

and other trace GHGs amplify CO_2 forcing by an additional 40%. f_{ESS} is 0.5 ± 0.25 (1σ), which assumes that the changes in ice, vegetation, and paleogeography amplify forcing by 50%. This value was informed by the average ratio between ESS and ECS from PlioMIP1 (1.5) (Haywood et al., 2013). The PlioMIP2 model simulations have a slightly higher mean ratio of 1.67 (Haywood et al., 2020); however, this mean value is skewed by one model with a ratio of 3.1. The median of the ensemble is 1.6, which is closer to the Sherwood et al. (2020) assumption. Finally, ζ is 0.06 ± 0.2 (1σ), based on long model runs which quantify the difference between true ECS and the shorter-term S (Sherwood et al., 2020).

ΔT represents the change in GMST during the mid-Pliocene relative to preindustrial conditions, which Sherwood et al. (2020) assumed was 3 ± 1°C (1σ). We update that here with the plioDA estimate of 4.1 ± 0.6°C (1σ), and solve Equation 3 for the net climate feedback, λ, from which climate sensitivity S can be computed from Equation 4. Following the Bayesian methodology of Sherwood et al. (2020), we then combine the resulting likelihood for S with a Uniform prior ($U[0, 20]$) to obtain a posterior estimate of S based solely on the Pliocene. Figure 7 displays the resulting probability distributions using both the Sherwood et al. (2020) ΔT and the plioDA ΔT. With the plioDA ΔT, S moves up 3.3°C (90% CI = 1.3°C–7.5°C) as given in Sherwood et al. (2020) to 4.8°C (90% CI = 2.6–9.9°C), implying higher ECS (based on the Pliocene alone) than previously thought. The lower bound of the plioDA 90% CI (2.6°C) is in good agreement with the lower bounds of the IPCC AR6 assessment (2°C–5°C) (Forster et al., 2021) and the Sherwood et al. (2020) posterior distribution (2.3°C–4.7°C; Figure 7) based on multiple lines of evidence (process understanding, historical data, and paleoclimate). The plioDA median falls near the upper bound of the 90% confidence interval of these estimates (Figure 7) indicating that a large portion of the plioDA probability distribution lies at the higher end of, or above, estimates of modern ECS. However, our results do not account for the "pattern effect," or rather, the impact that SST warming patterns have on climate feedbacks, and therefore climate sensitivity (Armour et al., 2013). Preferential warming in regions with tropical deep convection produces more negative feedbacks and reduces climate sensitivity, whereas warming in areas with reflective low clouds or sea ice leads leads to more positive feedbacks and higher climate sensitivity (Andrews & Webb, 2018; Dong et al., 2019). Accounting for the pattern effect in the Last Glacial Maximum reduced the range of modern ECS in Sherwood et al. (2020) to 2.1°C–4.1°C (Cooper et al., 2024), and similar accounting for the Pliocene could have a substantial impact on the inferred climate sensitivity here. Any impact would depend on how Pliocene SST patterns differ from those projected for CO_2 doubling, for example, due to the Pliocene's El Niño-like configuration of the tropical Pacific (Andrews & Webb, 2018; Dong et al., 2019) or its enhanced amplification of warming at higher latitudes (Cooper et al., 2024). Atmosphere-only model simulations are required to isolate the pattern effect, but if the Pliocene's unique SST pattern is responsible for the apparently high climate sensitivity, accounting for the pattern effect would adjust the probability

distribution down to lower values, as well as reduce the uncertainty (Cooper et al., 2024). Thus, while our estimate of ECS from the Pliocene is on face value higher than those for cold climates like the LGM (Cooper et al., 2024; Tierney et al., 2020), further work is needed to isolate the contribution of the pattern effect.

4.4. Hydroclimate and Implications for Ocean Circulation

plioDA-reconstructed $P - E$ is more sensitive to the choice of model prior than the temperature fields, with the cloud-only experiment showing different responses in the tropics and subtropics (Figure S7 in Supporting Information S1). This reflects the impact of model boundary conditions on the covariance structure between SST and hydroclimate, which determines how the SST changes are projected onto $P - E$. In the PlioMIP2-only and full prior reconstructions, the posterior patterns in $P - E$ are similar, suggesting that PlioMIP2 boundary conditions dominate the spatial patterns. Previous model sensitivity testing with CESM2 indicates that changes in the cryosphere and vegetation in particular are responsible for many of the large-scale features of Pliocene hydro-climatic change, such as for example, the elevated precipitation in the Afro-Asian monsoon region (Feng et al., 2022). This highlights the need for realistic boundary conditions to accurately simulate and reconstruct past hydroclimate change. In addition, the sensitivity of the plioDA $P - E$ results to the model prior choice is a reminder that assimilation of SST proxies provides a weaker constraint on posterior hydroclimate than temperature, and that the reconstructed fields should be interpreted cautiously. In other words, model physics have a strong influence on the spatial patterns of posterior hydroclimate fields.

In spite of the large differences across model prior choices, there are some features of plioDA $P - E$ that appear in all of the posterior solutions, and in some cases, are also distinct from both the PlioMIP2 and cloud prior means (Figure S9 in Supporting Information S1). For example, plioDA indicates an increase in $P - E$ the subtropical regions of south Africa and western North America (Figure 4a; Figure S9 in Supporting Information S1) in agreement with proxy evidence (N. J. Burls & Fedorov, 2017) and in spite of the fact that the PlioMIP2 multi-model mean does not show wetter conditions in these regions (Figure S9 in Supporting Information S1). The wetter conditions in western North America in particular are very different from the model priors (Figure S9 in Supporting Information S1) which, considering the strong evidence for positive water balance there (Ibarra et al., 2018), suggests that assimilation of SST data is updating the $P - E$ field in the right direction. However, the center of the increase in $P - E$ sits off of the Baja California Peninsula (Figure 4a) rather than on land, which, as discussed in Section 4.1, may reflect the fact that the North Pacific PDO-negative pattern produced by plioDA results in cooler SST anomalies on the California margin than the data suggest.

The plioDA posterior SSS reconstruction (Figure 4b) provides an integrated view on the effects of hydroclimatic change and circulation on the surface ocean. Compared to the prior mean change in SSS, plioDA shows stronger differences in the Atlantic, Pacific, and Indian ocean basins (Figures 8a and 8b). These include a large increase in SSS in the North Atlantic, a decrease in the North Pacific (particularly within the Gulf of Alaska and also off the California margin) and a decrease in the northern Indian Ocean (associated with the reconstructed intensification of the Indian monsoon, Figure 4a). The SSS posterior is somewhat more resilient to model prior choice than $P - E$, in that the large-scale pattern of a saltier Atlantic and fresher Pacific appears regardless of whether the PlioMIP or cloud simulations are used in the prior (Figure S7 in Supporting Information S1). However, there are regional differences that, like $P - E$, relate to the Pliocene boundary conditions. For example, the large increase in salinity in the North Atlantic in plioDA seems diagnostic of the closure of the Arctic gateways, which restricts freshwater export to the North Atlantic (Brierley & Fedorov, 2016). The PlioMIP2-only prior produces a salty North Atlantic, but with the cloud-only prior, the North Atlantic is actually fresher, since those simulations have the gateways open (Figure S7 in Supporting Information S1). However, in the North Pacific, assimilation of the SST proxies results in fresher conditions no matter the prior choice (Figure S7 in Supporting Information S1). This is because all of the posterior solutions for $P - E$ show an invigorated Pacific storm track (manifest as positive $P - E$ in the subpolar gyre and along the Gulf of Alaska) and a stronger Indian-Asian monsoon system, two major components of the North Pacific salinity balance (Emile-Geay et al., 2003) (Figure S7 in Supporting Information S1). Apparently, these particular changes in hydroclimate are less sensitive to boundary conditions, such as the status of the gateways, the cryosphere, or vegetative cover.

Previous work has argued that a Pacific Meridional Overturning Circulation (PMOC) existed during the mid-Pliocene (N. J. Burls et al., 2017; Ford et al., 2022; Shankle et al., 2021), partly on the basis of the model simulation shown in Figure 8c, an idealized "cloud" simulation (plioB17) that is part of our model prior. This

a. Prior mean

b. plioDA
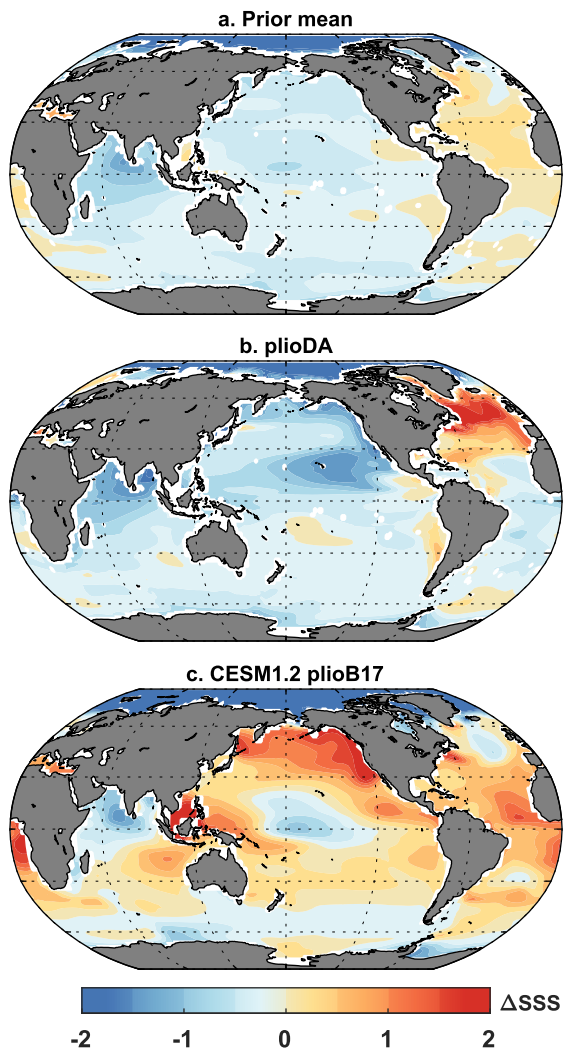
c. CESM1.2 plioB17

Figure 8. mid-Pliocene−preindustrial changes in sea-surface salinity (ΔSSS) in (a). The model prior mean, (b) the plioDA mid-Pliocene reconstruction, and (c) an early Pliocene-like simulation (plioB17) with CESM1.2 that produces Pacific Meridional Overturning Circulation (Ford et al., 2022).

simulation was conducted under modern boundary conditions, including preindustrial levels of CO_2, yet features a GMST increase (relative to the control simulation) of 5.2°C due to an imposed increase in tropical albedo of 0.073 and decrease in extratropical albedo of −0.039 (N. Burls & Fedorov, 2014). In this simulation, the change in $P - E$ is negative in the North Pacific and moisture transport to the region is reduced (N. J. Burls et al., 2017). This leads to a saltier North Pacific and fresher North Atlantic, resulting in weaker AMOC and active PMOC (N. J. Burls et al., 2017).

The results from plioDA in North Atlantic and North Pacific are nearly the opposite of the plioB17 simulation (Figures 8b and 8c). With an active PMOC, plioB17 simulates an increase in North Pacific SSTs (including near the Kamchatka Peninsula and within the Gulf of Alaska) of 8°C–10°C (N. J. Burls et al., 2017) (their Figure 4c), but the SST proxies (Figure 1), and thus plioDA (Figure 3a), show no such anomaly. Rather, the SST proxies show minimal warming in the North Pacific subpolar region, and enhanced warming in the North Atlantic, which supports a stronger AMOC during the Pliocene (in accordance with gateway closure, Otto-Bliesner et al. (2017)). Meanwhile, surface freshening of the subpolar North Pacific would disfavor convection and deep water formation. Thus, plioDA fundamentally contradicts the hypothesis that North Pacific Deepwater formation, and in turn a PMOC, was active during the Pliocene.

Further research, and potentially alternative explanations, are needed to bring the surface ocean proxy evidence (represented by plioDA) into alignment with biogeochemical proxies, which point toward higher export productivity and altered nutrient, pH, and sedimentary redox conditions in the mid-Pliocene North and equatorial Pacific, and have been interpreted as evidence for North Pacific Deepwater formation (N. J. Burls et al., 2017; Shankle et al., 2021; Ford et al., 2022; Abell & Winckler, 2023). Perhaps more vigorous seasonal mixing, shifts in the characteristics of deep southern-sourced waters, or fundamental changes in the preformed nutrient content of North Pacific intermediate waters, could explain the biogeochemical data. In addition, new SST records from the center of the North Pacific will be critical to confirm whether the muted warming indicated by the data available thus far is correct.

5. Conclusions

By blending proxy SST data with a wide, multi-model prior, plioDA provides a spatially complete view of both mid and early Pliocene climate change that is informed by geological evidence. We find that the assimilation of proxy data alters SST patterns of warming in key regions, including the North Atlantic, North Pacific, and tropical Pacific. plioDA indicates that the mid-Pliocene was warmer than previously thought, leading to a higher inferred climate sensitivity. The early Pliocene was even warmer, with a substantially reduced tropical Pacific gradient, suggesting that this time period was fundamentally different from the mid-Pliocene and deserves further study. plioDA also provides reconstructions of hydroclimate in the form of posterior $P - E$ and SSS fields. plioDA SSS shows that the North Atlantic was saltier and the North Pacific fresher, supporting Arctic gateway closure but contradicting North Pacific Deep Water formation and an active PMOC. plioDA thus raises questions about previously inferred connections between North Pacific ocean circulation and biogeochemistry. Future work is needed to reconcile ocean nutrient, redox, and productivity proxies with SST changes, validate the plioDA hydroclimate and salinity reconstructions, and also to investigate the enigmatic drivers of early Pliocene warmth.

Conflict of Interest

The authors declare no conflicts of interest relevant to this study.

Data Availability Statement

The plioDA reconstructed fields are publicly available from Zenodo (Tierney, 2024b): https://zenodo.org/doi/10.5281/zenodo.14532079. The proxy data and code to run and reproduce the Pliocene DA (Tierney, 2025) are publicly available in the pliocene-da GitHub repository: https://github.com/jesstierney/pliocene-da. The model output used for the DA are publicly available from Zenodo (Tierney, 2024a): https://zenodo.org/doi/10.5281/zenodo.11646735. The Pliocene DA uses DASH data assimilation software version 4.2.2 (J. King, 2023), available on GitHub: https://github.com/JonKing93/DASH.

References

Abell, J. T., & Winckler, G. (2023). Long-term variability in Pliocene North Pacific ocean export production and its implications for ocean circulation in a warmer world. *AGU Advances*, *4*(4), e2022AV000853. https://doi.org/10.1029/2022av000853

Abell, J. T., Winckler, G., Anderson, R. F., & Herbert, T. D. (2021). Poleward and weakened westerlies during Pliocene warmth. *Nature*, *589*(7840), 70–75. https://doi.org/10.1038/s41586-020-03062-1

Andrews, T., & Webb, M. J. (2018). The dependence of global cloud and lapse rate feedbacks on the spatial structure of tropical Pacific warming. *Journal of Climate*, *31*(2), 641–654. https://doi.org/10.1175/jcli-d-17-0087.1

Annan, J. D., Hargreaves, J. C., & Mauritsen, T. (2022). A new global surface temperature reconstruction for the Last Glacial Maximum. *Climate of the Past*, *18*(8), 1883–1896. https://doi.org/10.5194/cp-18-1883-2022

Annan, J. D., Hargreaves, J. C., Mauritsen, T., McClymont, E., & Ho, S. L. (2024). Can we reliably reconstruct the mid-Pliocene Warm Period with sparse data and uncertain models? *Climate of the Past*, *20*(9), 1989–1999. https://doi.org/10.5194/cp-20-1989-2024

Armour, K. C., Bitz, C. M., & Roe, G. H. (2013). Time-varying climate sensitivity from regional feedbacks. *Journal of Climate*, *26*(13), 4518–4534. https://doi.org/10.1175/jcli-d-12-00544.1

Baatsen, M. L., von der Heydt, A. S., Kliphuis, M. A., Oldeman, A. M., & Weiffenbach, J. E. (2022). Warm mid-pliocene conditions without high climate sensitivity: The CCSM4-utrecht (CESM 1.0. 5) contribution to the PlioMIP2. *Climate of the Past*, *18*(4), 657–679. https://doi.org/10.5194/cp-18-657-2022

Bhattacharya, T., Feng, R., Tierney, J. E., Rubbelke, C., Burls, N., Knapp, S., & Fu, M. (2022). Expansion and intensification of the North American monsoon during the pliocene. *AGU Advances*, *3*(6), e2022AV000757. https://doi.org/10.1029/2022av000757

Brassell, S. C., Eglinton, G., Marlowe, I., Pflaumann, U., & Sarnthein, M. (1986). Molecular stratigraphy: A new tool for climatic assessment. *Nature*, *320*(6058), 129–133. https://doi.org/10.1038/320129a0

Brierley, C. M., & Fedorov, A. V. (2016). Comparing the impacts of miocene–pliocene changes in inter-ocean gateways on climate: Central American seaway, Bering Strait, and Indonesia. *Earth and Planetary Science Letters*, *444*, 116–130. https://doi.org/10.1016/j.epsl.2016.03.010

Brierley, C. M., Fedorov, A. V., Liu, Z., Herbert, T. D., Lawrence, K. T., & LaRiviere, J. P. (2009). Greatly expanded tropical warm pool and weakened Hadley circulation in the early Pliocene. *Science*, *323*(5922), 1714–1718. https://doi.org/10.1126/science.1167625

Burls, N., & Fedorov, A. (2014). What controls the mean east–west sea surface temperature gradient in the equatorial Pacific: The role of cloud albedo. *Journal of Climate*, *27*(7), 2757–2778. https://doi.org/10.1175/jcli-d-13-00255.1

Burls, N. J., & Fedorov, A. V. (2017). Wetter subtropics in a warmer world: Contrasting past and future hydrological cycles. *Proceedings of the National Academy of Sciences*, *114*(49), 12888–12893. https://doi.org/10.1073/pnas.1703421114

Burls, N. J., Fedorov, A. V., Sigman, D. M., Jaccard, S. L., Tiedemann, R., & Haug, G. H. (2017). Active Pacific meridional overturning circulation (PMOC) during the warm Pliocene. *Science Advances*, *3*(9), e1700156. https://doi.org/10.1126/sciadv.1700156

Chan, W.-L., & Abe-Ouchi, A. (2020). Pliocene model Intercomparison project (PlioMIP2) simulations using the model for interdisciplinary research on climate (MIROC4m). *Climate of the Past*, *16*(4), 1523–1545. https://doi.org/10.5194/cp-16-1523-2020

Chandan, D., & Peltier, W. R. (2017). Regional and global climate for the mid-Pliocene using the University of Toronto version of CCSM4 and PlioMIP2 boundary conditions. *Climate of the Past*, *13*(7), 919–942. https://doi.org/10.5194/cp-13-919-2017

Cooper, V., Armour, K. C., Hakim, G. J., Tierney, J. E., Osman, M. B., Proistosescu, C., et al. (2024). Last Glacial Maximum pattern effects reduce climate sensitivity estimates. *Science Advances*, *10*(16). https://doi.org/10.1126/sciadv.adk9461

Cronblad, H. G., & Malmgren, B. A. (1981). Climatically controlled variation of Sr and Mg in Quaternary planktonic foraminifera. *Nature*, *291*(5810), 61–64. https://doi.org/10.1038/291061a0

De La Vega, E., Chalk, T. B., Wilson, P. A., Bysani, R. P., & Foster, G. L. (2020). Atmospheric CO_2 during the mid-piacenzian warm period and the M2 glaciation. *Scientific Reports*, *10*(1), 1–8.

Dekens, P. S., Ravelo, A. C., & McCarthy, M. D. (2007). Warm upwelling regions in the Pliocene warm period. *Paleoceanography*, *22*(3). https://doi.org/10.1029/2006pa001394

Dong, Y., Proistosescu, C., Armour, K. C., & Battisti, D. S. (2019). Attributing historical and future evolution of radiative feedbacks to regional warming patterns using a Green's function approach: The preeminence of the western Pacific. *Journal of Climate*, *32*(17), 5471–5491. https://doi.org/10.1175/jcli-d-18-0843.1

Dowsett, H., Barron, J., & Poore, R. (1996). Middle Pliocene sea surface temperatures: A global reconstruction. *Marine Micropaleontology*, *27*(1–4), 13–25. https://doi.org/10.1016/0377-8398(95)00050-x

Dowsett, H., Dolan, A., Rowley, D., Moucha, R., Forte, A. M., Mitrovica, J. X., et al. (2016). The PRISM4 (mid-Piacenzian) paleoenvironmental reconstruction. *Climate of the Past*, *12*(7), 1519–1538. https://doi.org/10.5194/cp-12-1519-2016

Dowsett, H., Robinson, M., Haywood, A., Salzmann, U., Hill, D., Sohl, L., et al. (2010). The PRISM3D paleoenvironmental reconstruction. *Stratigraphy*, *7*(2–3), 123–139. https://doi.org/10.29041/strat.07.2.03

Dutton, A., Carlson, A. E., Long, A. J., Milne, G. A., Clark, P. U., DeConto, R., et al. (2015). Sea-level rise due to polar ice-sheet mass loss during past warm periods. *Science*, *349*(6244), aaa4019. https://doi.org/10.1126/science.aaa4019

Emile-Geay, J., Cane, M. A., Naik, N., Seager, R., Clement, A. C., & van Geen, A. (2003). Warren revisited: Atmospheric freshwater fluxes and "Why is no deep water formed in the North Pacific". *Journal of Geophysical Research*, *108*(C6). https://doi.org/10.1029/2001jc001058

Erfani, E., & Burls, N. J. (2019). The strength of low-cloud feedbacks and tropical climate: A CESM sensitivity study. *Journal of Climate*, *32*(9), 2497–2516. https://doi.org/10.1175/jcli-d-18-0551.1

Evans, D., & Müller, W. (2012). Deep time foraminifera Mg/Ca paleothermometry: Nonlinear correction for secular change in seawater Mg/Ca. *Paleoceanography*, *27*(4). https://doi.org/10.1029/2012pa002315

Fedorov, A. V., Brierley, C., Lawrence, K. T., Liu, Z., Dekens, P., & Ravelo, A. (2013). Patterns and mechanisms of early Pliocene warmth. *Nature*, *496*(7443), 43–49. https://doi.org/10.1038/nature12003

Fedorov, A. V., Burls, N. J., Lawrence, K. T., & Peterson, L. C. (2015). Tightly linked zonal and meridional sea surface temperature gradients over the past five million years. *Nature Geoscience*, *8*(12), 975–980. https://doi.org/10.1038/ngeo2577

Feng, R., Bhattacharya, T., Otto-Bliesner, B. L., Brady, E. C., Haywood, A. M., Tindall, J. C., et al. (2022). Past terrestrial hydroclimate sensitivity controlled by Earth system feedbacks. *Nature Communications*, *13*(1), 1306. https://doi.org/10.1038/s41467-022-28814-7

Feng, R., Otto-Bliesner, B. L., Brady, E. C., & Rosenbloom, N. (2020). Increased climate response and Earth system sensitivity from CCSM4 to CESM2 in mid-Pliocene simulations. *Journal of Advances in Modeling Earth Systems*, *12*(8), e2019MS002033. https://doi.org/10.1029/2019ms002033

Ford, H. L., Burls, N. J., Jacobs, P., Jahn, A., Caballero-Gill, R. P., Hodell, D. A., & Fedorov, A. (2022). Sustained mid-Pliocene warmth led to deep water formation in the North Pacific. *Nature Geoscience*, *15*(8), 658–663. https://doi.org/10.1038/s41561-022-00978-3

Forster, P., Storelvmo, T., Armour, K., Collins, W., Dufresne, J.-L., Frame, D., et al. (2021). The Earth's energy budget, climate feedbacks, and climate sensitivity. In V. Masson-Delmotte, et al. (Eds.), *Climate change 2021: The physical science basis. Contribution of working group I to the sixth assessment report of the intergovernmental panel on climate change* (pp. 923–1054). Cambridge University Press.

Fu, M., Cane, M. A., Molnar, P., & Tziperman, E. (2022). Warmer pliocene upwelling site SST leads to wetter subtropical coastal areas: A positive feedback on SST. *Paleoceanography and Paleoclimatology*, *37*(2), e2021PA004357. https://doi.org/10.1029/2021pa004357

Golledge, N. R., Thomas, Z. A., Levy, R. H., Gasson, E. G., Naish, T. R., McKay, R. M., et al. (2017). Antarctic climate and ice-sheet configuration during the early Pliocene interglacial at 4.23 Ma. *Climate of the Past*, *13*(7), 959–975. https://doi.org/10.5194/cp-13-959-2017

Goosse, H., Kay, J. E., Armour, K. C., Bodas-Salcedo, A., Chepfer, H., Docquier, D., et al. (2018). Quantifying climate feedbacks in Polar Regions. *Nature Communications*, *9*(1), 1919. https://doi.org/10.1038/s41467-018-04173-0

Gothmann, A. M., Stolarski, J., Adkins, J. F., Schoene, B., Dennis, K. J., Schrag, D. P., et al. (2015). Fossil corals as an archive of secular variations in seawater chemistry since the Mesozoic. *Geochimica et Cosmochimica Acta*, *160*, 188–208. https://doi.org/10.1016/j.gca.2015.03.018

Grant, G., Naish, T., Dunbar, G., Stocchi, P., Kominz, M., Kamp, P. J., et al. (2019). The amplitude and origin of sea-level variability during the Pliocene epoch. *Nature*, *574*(7777), 237–241. https://doi.org/10.1038/s41586-019-1619-z

Gray, W. R., & Evans, D. (2019). Nonthermal influences on Mg/Ca in planktonic foraminifera: A review of culture studies and application to the last glacial maximum. *Paleoceanography and Paleoclimatology*, *34*(3), 306–315. https://doi.org/10.1029/2018pa003517

Guillermic, M., Misra, S., Eagle, R., & Tripati, A. (2022). Atmospheric CO_2 estimates for the Miocene to Pleistocene based on foraminiferal $\delta^{11}B$ at ocean drilling program sites 806 and 807 in the western equatorial pacific. *Climate of the Past*, *18*(2), 183–207. https://doi.org/10.5194/cp-18-183-2022

Gulev, S., Thorne, P., Ahn, J., Dentener, F., Domingues, C., Gerland, S., et al. (2021). Changing state of the climate system. In V. Masson-Delmotte, et al. (Eds.), *Climate change 2021: The physical science basis. contribution of working group i to the sixth assessment report of the intergovernmental panel on climate change* (pp. 287–422). Cambridge University Press.

Hahn, L. C., Armour, K. C., Zelinka, M. D., Bitz, C. M., & Donohoe, A. (2021). Contributions to polar amplification in CMIP5 and CMIP6 models. *Frontiers in Earth Science*, *9*, 710036. https://doi.org/10.3389/feart.2021.710036

Hakim, G. J., Emile-Geay, J., Steig, E. J., Noone, D., Anderson, D. M., Tardif, R., et al. (2016). The last millennium climate reanalysis project: Framework and first results. *Journal of Geophysical Research: Atmospheres*, *121*(12), 6745–6764. https://doi.org/10.1002/2016jd024751

Hall, J. R., Allison, M. S., Papadopoulos, M. T., Barfod, D. N., & Jones, S. M. (2023). Timing and consequences of Bering Strait opening: New insights from 40Ar/39Ar dating of the barmur group (tjörnes beds), northern Iceland. *Paleoceanography and Paleoclimatology*, *38*(4), e2022PA004539. https://doi.org/10.1029/2022pa004539

Haywood, A. M., Hill, D., Dolan, A., Otto-Bliesner, B. L., Bragg, F., Chan, W.-L., et al. (2013). Large-scale features of pliocene climate: Results from the pliocene model Intercomparison project. *Climate of the Past*, *9*(1), 191–209. https://doi.org/10.5194/cp-9-191-2013

Haywood, A. M., Tindall, J. C., Burton, L., Chandler, M., Dolan, A. M., Dowsett, H. J., et al. (2024). Pliocene model Intercomparison project phase 3 (PlioMIP3)–Science plan and experimental design. *Global and Planetary Change*, *232*, 104316. https://doi.org/10.1016/j.gloplacha.2023.104316

Haywood, A. M., Tindall, J. C., Dowsett, H. J., Dolan, A. M., Foley, K. M., Hunter, S. J., et al. (2020). The pliocene model Intercomparison project phase 2: Large-scale climate features and climate sensitivity. *Climate of the Past*, *16*(6), 2095–2123. https://doi.org/10.5194/cp-16-2095-2020

Hunter, S. J., Haywood, A. M., Dolan, A. M., & Tindall, J. C. (2019). The HadCM3 contribution to PlioMIP phase 2. *Climate of the Past*, *15*(5), 1691–1713. https://doi.org/10.5194/cp-15-1691-2019

Ibarra, D. E., Oster, J. L., Winnick, M. J., Caves Rugenstein, J. K., Byrne, M. P., & Chamberlain, C. P. (2018). Warm and cold wet states in the western United States during the Pliocene–Pleistocene. *Geology*, *46*(4), 355–358. https://doi.org/10.1130/g39962.1

King, J. (2023). Dash. (Version 4.2.2) [Code]. *Zenodo*. Retrieved from https://doi.org/10.5281/zenodo.8277407

King, J. M., Tierney, J., Osman, M., Judd, E. J., & Anchukaitis, K. J. (2023). *Dash: A matlab toolbox for paleoclimate data assimilation* (Vol. 1–46). EGUsphere.

Koenig, S., Dolan, A., De Boer, B., Stone, E., Hill, D., DeContoAbe-OuchiConto, R. M. A. R., et al. (2015). Ice sheet model dependency of the simulated Greenland Ice Sheet in the mid-Pliocene. *Climate of the Past*, *11*(3), 369–381. https://doi.org/10.5194/cp-11-369-2015

Lauvset, S. K., Key, R. M., Olsen, A., Van Heuven, S., Velo, A., Lin, X., et al. (2016). A new global interior ocean mapped climatology: The 1 $\times$ 1 GLODAP version 2. *Earth System Science Data*, *8*(2), 325–340. https://doi.org/10.5194/essd-8-325-2016

Li, X., Guo, C., Zhang, Z., Otterå, O. H., & Zhang, R. (2020). PlioMIP2 simulations with NorESM-L and NorESM1-F. *Climate of the Past*, *16*(1), 183–197. https://doi.org/10.5194/cp-16-183-2020

Lunt, D. J., Haywood, A. M., Schmidt, G. A., Salzmann, U., Valdes, P. J., Dowsett, H. J., & Loptson, C. A. (2012). On the causes of mid-Pliocene warmth and polar amplification. *Earth and Planetary Science Letters*, *321*, 128–138. https://doi.org/10.1016/j.epsl.2011.12.042

Lurton, T., Balkanski, Y., Bastrikov, V., Bekki, S., Bopp, L., Braconnot, P., et al. (2020). Implementation of the CMIP6 forcing data in the IPSL-cm6a-LR model. *Journal of Advances in Modeling Earth Systems*, *12*(4), e2019MS001940. https://doi.org/10.1029/2019ms001940

Mantua, N. J., Hare, S. R., Zhang, Y., Wallace, J. M., & Francis, R. C. (1997). A Pacific interdecadal climate oscillation with impacts on salmon production. *Bulletin of the American Meteorological Society*, *78*(6), 1069–1080. https://doi.org/10.1175/1520-0477(1997)078<1069:apicow>2.0.co;2

Marincovich, L., Jr., & Gladenkov, A. Y. (1999). Evidence for an early opening of the Bering Strait. *Nature*, *397*(6715), 149–151. https://doi.org/10.1038/16446

McClymont, E. L., Ford, H. L., Ho, S. L., Tindall, J. C., Haywood, A. M., Alonso-Garcia, M., et al. (2020). Lessons from a high-CO_2 world: An ocean view from $\sim$ 3 million years ago. *Climate of the Past*, *16*(4), 1599–1615. https://doi.org/10.5194/cp-16-1599-2020

McClymont, E. L., Ho, S.-L., Ford, H., Bailey, I., Berke, M. A., Bolton, C. T., et al. (2023). Climate evolution through the onset and intensification of northern Hemisphere glaciation. *Reviews of Geophysics*, *61*(3), e2022RG000793. https://doi.org/10.1029/2022rg000793

McGirr, R., Seton, M., & Williams, S. (2021). Kinematic and geodynamic evolution of the isthmus of Panama region: Implications for central American seaway closure. *GSA Bulletin*, *133*(3–4), 867–884. https://doi.org/10.1130/b35595.1

Meinicke, N., Reimi, M. A., Ravelo, A., & Meckler, A. N. (2021). Coupled Mg/Ca and clumped isotope measurements indicate lack of substantial mixed layer cooling in the Western Pacific Warm Pool during the last $\sim$ 5 million years. *Paleoceanography and Paleoclimatology*, *36*(8), e2020PA004115. https://doi.org/10.1029/2020pa004115

Müller, R. D., Cannon, J., Qin, X., Watson, R. J., Gurnis, M., Williams, S., et al. (2018). Gplates: Building a virtual earth through deep time. *Geochemistry, Geophysics, Geosystems*, *19*(7), 2243–2261. https://doi.org/10.1029/2018gc007584

Müller, R. D., Zahirovic, S., Williams, S. E., Cannon, J., Seton, M., Bower, D. J., et al. (2019). A global plate model including lithospheric deformation along major rifts and orogens since the triassic. *Tectonics*, *38*(6), 1884–1907. https://doi.org/10.1029/2018tc005462

Newman, M., Alexander, M. A., Ault, T. R., Cobb, K. M., Deser, C., Di Lorenzo, E., et al. (2016). The Pacific decadal oscillation, revisited. *Journal of Climate*, *29*(12), 4399–4427. https://doi.org/10.1175/jcli-d-15-0508.1

O'Brien, C. L., Foster, G. L., Martínez-Botí, M. A., Abell, R., Rae, J. W., & Pancost, R. D. (2014). High sea surface temperatures in tropical warm pools during the Pliocene. *Nature Geoscience*, *7*(8), 606–611. https://doi.org/10.1038/ngeo2194

O'Dea, A., Lessios, H. A., Coates, A. G., Eytan, R. I., Restrepo-Moreno, S. A., Cione, A. L., et al. (2016). Formation of the isthmus of Panama. *Science Advances*, *2*(8), e1600883. https://doi.org/10.1126/sciadv.1600883

Osman, M. B., Tierney, J. E., Zhu, J., Tardif, R., Hakim, G. J., King, J., & Poulsen, C. J. (2021). Globally resolved surface temperatures since the last glacial maximum. *Nature*, *599*(7884), 239–244. https://doi.org/10.1038/s41586-021-03984-4

Otto-Bliesner, B. L., Jahn, A., Feng, R., Brady, E. C., Hu, A., & Löfverström, M. (2017). Amplified North atlantic warming in the late pliocene by changes in arctic gateways. *Geophysical Research Letters*, *44*(2), 957–964. https://doi.org/10.1002/2016gl071805

PALAEOSENS Project Members. (2012). Making sense of palaeoclimate sensitivity. *Nature*, *491*(7426), 683–691. https://doi.org/10.1038/nature11574

Rayner, N., Parker, D. E., Horton, E., Folland, C. K., Alexander, L. V., Rowell, D., et al. (2003). Global analyses of sea surface temperature, sea ice, and night marine air temperature since the late nineteenth century. *Journal of Geophysical Research*, *108*(D14). https://doi.org/10.1029/2002jd002670

Rosenthal, Y., Bova, S., & Zhou, X. (2022). A user guide for choosing planktic foraminiferal Mg/Ca-temperature calibrations. *Paleoceanography and Paleoclimatology*, *37*(6), e2022PA004413. https://doi.org/10.1029/2022pa004413

Rubbelke, C. B., Bhattacharya, T., Feng, R., Burls, N. J., Knapp, S., & McClymont, E. L. (2023). Plio-pleistocene southwest african hydroclimate modulated by benguela and Indian ocean temperatures. *Geophysical Research Letters*, *50*(19), e2023GL103003. https://doi.org/10.1029/2023gl103003

Salzmann, U., Dolan, A. M., Haywood, A. M., Chan, W.-L., Voss, J., Hill, D. J., et al. (2013). Challenges in quantifying Pliocene terrestrial warming revealed by data–model discord. *Nature Climate Change*, *3*(11), 969–974. https://doi.org/10.1038/nclimate2008

Schouten, S., Hopmans, E. C., Schefuß, E., & Damste, J. S. S. (2002). Distributional variations in marine crenarchaeotal membrane lipids: A new tool for reconstructing ancient sea water temperatures? *Earth and Planetary Science Letters*, *204*(1–2), 265–274. https://doi.org/10.1016/s0012-821x(02)00979-2

Shankle, M. G., Burls, N. J., Fedorov, A. V., Thomas, M. D., Liu, W., Penman, D. E., et al. (2021). Pliocene decoupling of equatorial Pacific temperature and pH gradients. *Nature*, *598*(7881), 457–461. https://doi.org/10.1038/s41586-021-03884-7

Sherwood, S. C., Webb, M. J., Annan, J. D., Armour, K. C., Forster, P. M., Hargreaves, J. C., et al. (2020). An assessment of Earth's climate sensitivity using multiple lines of evidence. *Reviews of Geophysics*, *58*(4), e2019RG000678. https://doi.org/10.1029/2019rg000678

Smith, D. M., Screen, J. A., Deser, C., Cohen, J., Fyfe, J. C., García-Serrano, J., et al. (2019). The polar amplification model Intercomparison project (PAMIP) contribution to CMIP6: Investigating the causes and consequences of polar amplification. *Geoscientific Model Development*, *12*(3), 1139–1164. https://doi.org/10.5194/gmd-12-1139-2019

Sosdian, S. M., Greenop, R., Hain, M., Foster, G. L., Pearson, P. N., & Lear, C. H. (2018). Constraining the evolution of Neogene ocean carbonate chemistry using the boron isotope pH proxy. *Earth and Planetary Science Letters*, *498*, 362–376. https://doi.org/10.1016/j.epsl.2018.06.017

Stepanek, C., Samakinwa, E., Knorr, G., & Lohmann, G. (2020). Contribution of the coupled atmosphere–ocean–sea ice–vegetation model COSMOS to the PlioMIP2. *Climate of the Past*, *16*(6), 2275–2323. https://doi.org/10.5194/cp-16-2275-2020

Tan, N., Contoux, C., Ramstein, G., Sun, Y., Dumas, C., Sepulchre, P., & Guo, Z. (2020). Modeling a modern-like p CO_2 warm period (Marine Isotope Stage KM5c) with two versions of an Institut Pierre Simon Laplace atmosphere–ocean coupled general circulation model. *Climate of the Past*, *16*(1), 1–16. https://doi.org/10.5194/cp-16-1-2020

Tanner, T., Hernández-Almeida, I., Drury, A. J., Guitián, J., & Stoll, H. (2020). Decreasing atmospheric CO_2 during the late Miocene cooling. *Paleoceanography and Paleoclimatology*, *35*(12), e2020PA003925. https://doi.org/10.1029/2020pa003925

Tierney, J. E. (2024a). plioDA model simulation prior (version 1) [Dataset]. *Zenodo*. Retrieved from https://doi.org/10.5281/zenodo.11646736

Tierney, J. E. (2024b). plioDA reconstructed climate fields (version 1.0) [Dataset]. *Zenodo*. Retrieved from https://doi.org/10.5281/zenodo.14532078

Tierney, J. E. (2025). Pliocene-da (version 1.0) [code]. *Zenodo*. Retrieved from https://doi.org/10.5281/zenodo.14635811

Tierney, J. E., Haywood, A. M., Feng, R., Bhattacharya, T., & Otto-Bliesner, B. L. (2019a). Pliocene warmth consistent with greenhouse gas forcing. *Geophysical Research Letters*, *46*(15), 9136–9144. https://doi.org/10.1029/2019gl083802

Tierney, J. E., Malevich, S. B., Gray, W., Vetter, L., & Thirumalai, K. (2019b). Bayesian calibration of the Mg/Ca paleothermometer in planktic foraminifera. *Paleoceanography and Paleoclimatology*, *34*(12), 2005–2030. https://doi.org/10.1029/2019pa003744

Tierney, J. E., & Tingley, M. P. (2014). A Bayesian, spatially-varying calibration model for the TEX_{86} proxy. *Geochimica et Cosmochimica Acta*, *127*, 83–106. https://doi.org/10.1016/j.gca.2013.11.026

Tierney, J. E., & Tingley, M. P. (2018). Bayspline: A new calibration for the alkenone paleothermometer. *Paleoceanography and Paleoclimatology*, *33*(3), 281–301. https://doi.org/10.1002/2017pa003201

Tierney, J. E., Zhu, J., King, J., Malevich, S. B., Hakim, G. J., & Poulsen, C. J. (2020). Glacial cooling and climate sensitivity revisited. *Nature*, *584*(7822), 569–573. https://doi.org/10.1038/s41586-020-2617-x

Tierney, J. E., Zhu, J., Li, M., Ridgwell, A., Hakim, G. J., Poulsen, C. J., et al. (2022). Spatial patterns of climate change across the paleocene–eocene thermal maximum. *Proceedings of the National Academy of Sciences*, *119*(42), e2205326119. https://doi.org/10.1073/pnas.2205326119

Vallejo-Hincapié, F., Pardo-Trujillo, A., Barbosa-Espitia, Á., Aguirre, D., Celis, S. A., Giraldo-Villegas, C. A., et al. (2024). *Miocene vanishing of the central American seaway between the panamá arc and the south American plate*. Geological Society of America Bulletin.

Wara, M. W., Ravelo, A. C., & Delaney, M. L. (2005). Permanent El niño-like conditions during the pliocene warm period. *Science*, *309*(5735), 758–761. https://doi.org/10.1126/science.1112596

Weiffenbach, J. E., Baatsen, M. L., Dijkstra, H. A., Von Der Heydt, A. S., Abe-Ouchi, A., Brady, E. C., et al. (2023). Unraveling the mechanisms and implications of a stronger mid-pliocene atlantic meridional overturning circulation (AMOC) in PlioMIP2. *Climate of the Past*, *19*(1), 61–85. https://doi.org/10.5194/cp-19-61-2023

Williams, C. J., Sellar, A. A., Ren, X., Haywood, A. M., Hopcroft, P., Hunter, S. J., et al. (2021). Simulation of the mid-pliocene warm period using HadGEM3: Experimental design and results from model–model and model–data comparison. *Climate of the Past*, *17*(5), 2139–2163. https://doi.org/10.5194/cp-17-2139-2021

Zhang, Q., Berntell, E., Axelsson, J., Chen, J., Han, Z., De Nooijer, W., et al. (2021). Simulating the mid-Holocene, last interglacial and mid-Pliocene climate with EC-Earth3-LR. *Geoscientific Model Development*, *14*(2), 1147–1169. https://doi.org/10.5194/gmd-14-1147-2021

Zhang, Y. G., Pagani, M., & Liu, Z. (2014). A 12-million-year temperature history of the tropical Pacific Ocean. *Science*, *344*(6179), 84–87. https://doi.org/10.1126/science.1246172

Zhou, X., Rosenthal, Y., Haynes, L., Si, W., Evans, D., Huang, K.-F., et al. (2021). Planktic foraminiferal Na/Ca: A potential proxy for seawater calcium concentration. *Geochimica et Cosmochimica Acta*, *305*, 306–322. https://doi.org/10.1016/j.gca.2021.04.012

References From the Supporting Information

Delaney, M. L., Bé, A. W., & Boyle, E. A. (1985). Li, Sr, Mg, and Na in foraminiferal calcite shells from laboratory culture, sediment traps, and sediment cores. *Geochimica et Cosmochimica Acta*, *49*(6), 1327–1341. https://doi.org/10.1016/0016-7037(85)90284-4

Evans, D., Brierley, C., Raymo, M. E., Erez, J., & Müller, W. (2016). Planktic foraminifera shell chemistry response to seawater chemistry: Pliocene–Pleistocene seawater Mg/Ca, temperature and sea level change. *Earth and Planetary Science Letters*, *438*, 139–148. https://doi.org/10.1016/j.epsl.2016.01.013

Evans, D., Erez, J., Oron, S., & Müller, W. (2015). Mg/Ca-temperature and seawater-test chemistry relationships in the shallow-dwelling large benthic foraminifera Operculina ammonoides. *Geochimica et Cosmochimica Acta*, *148*, 325–342. https://doi.org/10.1016/j.gca.2014.09.039

Hauzer, H., Evans, D., Müller, W., Rosenthal, Y., & Erez, J. (2018). Calibration of Na partitioning in the calcitic foraminifer Operculina ammonoides under variable Ca concentration: Toward reconstructing past seawater composition. *Earth and Planetary Science Letters*, *497*, 80–91. https://doi.org/10.1016/j.epsl.2018.06.004

Holland, K., Branson, O., Haynes, L. L., Hönisch, B., Allen, K. A., Russell, A. D., et al. (2020). Constraining multiple controls on planktic foraminifera Mg/Ca. *Geochimica et Cosmochimica Acta*, *273*, 116–136. https://doi.org/10.1016/j.gca.2020.01.015

Mucci, A., & Morse, J. W. (1983). The incorporation of Mg^{2+} and Sr^{2+} into calcite overgrowths: Influences of growth rate and solution composition. *Geochimica et Cosmochimica Acta*, *47*(2), 217–233. https://doi.org/10.1016/0016-7037(83)90135-7

Segev, E., & Erez, J. (2006). Effect of Mg/Ca ratio in seawater on shell composition in shallow benthic foraminifera. *Geochemistry, Geophysics, Geosystems*, *7*(2). https://doi.org/10.1029/2005gc000969

Ternois, Y., Sicre, M.-A., Boireau, A., Marty, J.-C., & Miquel, J.-C. (1996). Production pattern of alkenones in the mediterranean sea. *Geophysical Research Letters*, *23*(22), 3171–3174. https://doi.org/10.1029/96gl02910